HHS Public Access

Author manuscript

Nature. Author manuscript; available in PMC 2024 December 01.

Published in final edited form as:

Nature. 2024 June ; 630(8016): 437–446. doi:10.1038/s41586-024-07373-5.

ROS-dependent *S*-palmitoylation activates cleaved and intact gasdermin D

Gang Du[1,2,13,✉], **Liam B. Healy**[1,2,13], **Liron David**[1,2,12,✉], **Caitlin Walker**[1,2,11], **Tarick J. El-Baba**[3,4], **Corinne A. Lutomski**[3,4], **Byoungsook Goh**[5], **Bowen Gu**[2,6], **Xiong Pi**[1,2], **Pascal Devant**[7], **Pietro Fontana**[1,2], **Ying Dong**[1,2], **Xiyu Ma**[2,6], **Rui Miao**[2,6], **Arumugam Balasubramanian**[8,9], **Robbins Puthenveetil**[10], **Anirban Banerjee**[10], **Hongbo R. Luo**[8,9], **Jonathan C. Kagan**[7], **Sungwhan F. Oh**[5], **Carol V. Robinson**[3,4], **Judy Lieberman**[2,6], **Hao Wu**[1,2,✉]

[1]Department of Biological Chemistry and Molecular Pharmacology, Harvard Medical School, Boston, MA, USA.

[2]Program in Cellular and Molecular Medicine, Boston Children's Hospital, Boston, MA, USA.

[3]Department of Chemistry, University of Oxford, Oxford, UK.

[4]Kavli Institute for NanoScience Discovery, University of Oxford, Oxford, UK.

[5]Center for Experimental Therapeutics and Reperfusion Injury, Department of Anesthesiology, Perioperative and Pain Medicine, Brigham and Women's Hospital, Boston, MA, USA.

[6]Department of Pediatrics, Harvard Medical School, Boston, MA, USA.

[7]Harvard Medical School and Division of Gastroenterology, Boston Children's Hospital, Boston, MA, USA.

[✉]**Correspondence and requests for materials** should be addressed to Gang Du, Liron David or Hao Wu. gdu@crystal.harvard.edu; david@crystal.harvard.edu; wu@crystal.harvard.edu.

[13]These authors contributed equally: Gang Du, Liam B. Healy.

Author contributions H.W., G.D., L.B.H., L.D., C.W. and J.L. conceived the study. G.D. designed and performed most of the experiments. L.B.H. designed and performed most of the remaining experiments. T.J.E.-B. and C.A.L. designed and performed intact MS under C.V.R.'s supervision. B. Goh and G.D. designed and performed UPLC–MS/MS analysis with S.F.O. and H.W.'s supervision. B. Gu performed CRISPR–Cas9 knockout of *ZDHHC5* and *ZDHHC9* under J.L.'s supervision. P.D. prepared primary BMDMs under J.C.K.'s supervision. A. Balasubramanian and H.R.L. provided siRNAs for knocking down *ZDHHC* genes. X.P. helped with cryo-EM data processing for full-length GSDMD pore structure. P.F. and Y.D. helped with GSDMD and CASP1 expression, respectively. R.M. provided *Crls1*- or *Plscr3*-KO iBMDMs. X.M. attempted knock-in of the Halo tag to GSDMD in THP-1 cells. R.P. and A. Banerjee provided Heatil screen constructs. H.W., L.B.H., G.D. and J.L. wrote the manuscript with input from all of the authors.

Competing interests H.W. and J.L. are cofounders of Ventus Therapeutics. J.C.K. consults and holds equity in Corner Therapeutics, Larkspur Biosciences, MindImmune Therapeutics and Neumora Therapeutics. None of these relationships impacted this study. The other authors declare no competing interests.

Reporting summary

Further information on research design is available in the Nature Portfolio Reporting Summary linked to this article.

Additional information

Supplementary information The online version contains supplementary material available at https://doi.org/10.1038/s41586-024-07373-5.

Peer review information *Nature* thanks Françoise van der Goot and the other, anonymous, reviewer(s) for their contribution to the peer review of this work.

[8]Department of Pathology, Dana-Farber/Harvard Cancer Center, Harvard Medical School, Boston, MA, USA.

[9]Department of Laboratory Medicine, Boston Children's Hospital, Boston, MA, USA.

[10]Section on Structural and Chemical Biology, Neurosciences and Cellular and Structural Biology Division, Eunice Kennedy Shriver National Institute of Child Health and Human Development, National Institutes of Health, Bethesda, MD, USA.

[11]Present address: Department of Life Sciences, Ben-Gurion University of the Negev, Be'er Sheva, Israel.

[12]Present address: Seqirus, Cambridge, MA, USA.

Abstract

Gasdermin D (GSDMD) is the common effector for cytokine secretion and pyroptosis downstream of inflammasome activation and was previously shown to form large transmembrane pores after cleavage by inflammatory caspases to generate the GSDMD N-terminal domain (GSDMD-NT)[1–10]. Here we report that GSDMD Cys191 is *S*-palmitoylated and that palmitoylation is required for pore formation. *S*-palmitoylation, which does not affect GSDMD cleavage, is augmented by mitochondria-generated reactive oxygen species (ROS). Cleavage-deficient GSDMD (D275A) is also palmitoylated after inflammasome stimulation or treatment with ROS activators and causes pyroptosis, although less efficiently than palmitoylated GSDMD-NT. Palmitoylated, but not unpalmitoylated, full-length GSDMD induces liposome leakage and forms a pore similar in structure to GSDMD-NT pores shown by cryogenic electron microscopy. ZDHHC5 and ZDHHC9 are the major palmitoyltransferases that mediate GSDMD palmitoylation, and their expression is upregulated by inflammasome activation and ROS. The other human gasdermins are also palmitoylated at their N termini. These data challenge the concept that cleavage is the only trigger for GSDMD activation. They suggest that reversible palmitoylation is a checkpoint for pore formation by both GSDMD-NT and intact GSDMD that functions as a general switch for the activation of this pore-forming family.

GSDM-family proteins, which form cell-membrane pores to activate inflammatory cell death (pyroptosis) that release pro-inflammatory cytokines and alarmins, have key roles in host defence and homeostasis. GSDMD is activated by caspase cleavage[1–9], but all GSDMs can be activated by other host or microbial proteases in various physiological contexts[9,11]. These data established the paradigm that GSDMs are activated by proteolytic processing that separates the pore-forming NT from the autoinhibitory C-terminal domain (CT). Crystal structures of autoinhibited, full-length monomeric GSDMs[4,12] and cryogenic electron microscopy (cryo-EM) structures of GSDM-NTs in transmembrane pores or oligomeric prepores formed before membrane insertion[7,8] consolidated this paradigm. Here we demonstrate that GSDMD is modified at Cys191 of human GSDMD-NT (mouse Cys192) by reversible *S*-palmitoylation[13,14], which is enhanced by ROS-mediated[15] upregulation of palmitoyltransferases. Notably, GSDMD cleavage is not sufficient for cell death. Instead, palmitoylation is required for pore formation. Notably, palmitoylation of either GSDMD-NT or intact GSDMD triggers pore formation, identifying an ROS-related mechanism for activating this pore-forming family.

Palmitoylation of GSDMD Cys191 in pore formation

The C191A/C192A mutants of human/mouse GSDMD-NT are impaired in oligomerization and cell death induction[3], which cannot be explained by disulfide-bond formation[8,12] (Extended Data Fig. 1a,b). We tested whether GSDMD is *S*-palmitoylated at Cys191, which could explain why C191A is defective in pore formation. We used alkyne–azide click chemistry to determine whether GSDMD expressed in HEK293T cells could be metabolically labelled with palmitate or stearate[16] (Fig. 1a). Clicking with azido-biotin followed by Streptavidin pull-down (Fig. 1b) or rhodamine azide for direct visualization (Extended Data Fig. 1c) revealed robust GSDMD palmitoylation. Palmitoylation was greatly reduced by the non-specific palmitoylation inhibitor 2-bromopalmitate (2-BP)[17]. Click chemistry after metabolic labelling did not detect *N*-myristoylation of GSDMD despite a positive prediction[18] (Extended Data Fig. 1d).

S-palmitoylation is a type of *S*-acylation that can be detected using acyl–biotin exchange (ABE) or acyl–PEG exchange (APE), which detect acylated Cys residues by blocking unmodified Cys residues, removing acylation with hydroxylamine (HA), and biotinylating or attaching long polyethylene glycol (PEG) to free Cys residues[16] (Fig. 1c). With ABE, streptavidin pull-down revealed palmitoylation of HEK293T-expressed full-length GSDMD and GSDMD-NT, and the control palmitoylated protein calnexin, but not GSDMD-CT, which was blocked by 2-BP (Fig. 1d and Extended Data Fig. 1e,f). Acylation and lipid labelling confirmed palmitoylation—a term that does not necessarily imply a C16 lipid chain length. ABE revealed that other human GSDMs (A, B, C and E) expressed by HEK293T cells were all palmitoylated at the NT, and GSDME was also palmitoylated at the CT (Supplementary Fig. 1a–d), consistent with a previous report[19].

To identify the palmitoylated residue, GSDMD-NT constructs with each Cys mutated to Ala together with an I104N mutation (I105N in mouse), which slows GSDMD-NT pore formation[1,20], were expressed in HEK293T cells and analysed using ABE. All of the mutants behaved as the WT, except for the C191A mutant for which no palmitoylation was detected (Fig. 1e). Consistently, C191A compromised pyroptosis, as analysed by propidium iodide (PI) uptake, lactate dehydrogenase (LDH) release and an ATP luminescence cell viability assay, and reduced GSDMD-NT membrane localization on the basis of immunofluorescence analysis (Extended Data Fig. 1g–l). To test whether GSDMD-NT oligomerization depends on palmitoylation, lysates of GSDMD-NT-expressing HEK293T cells were analysed by non-reducing SDS–PAGE. GSDMD-NT oligomers were prominent in untreated lysates but absent after HA treatment to remove palmitoylation (Fig. 1f). By contrast, tris(2-carboxyethyl)phosphine (TCEP), which reduces disulfides but does not affect palmitoylation, did not affect oligomerization. As controls, WT GSDMD-NT expressed in HEK293T cells pretreated with 2-BP or co-transfected with short interfering RNAs (siRNAs) to knock down the palmitoyl acyl-transferases *ZDHHC5* and *ZDHHC9* that mediate GSDMD palmitoylation (see below) or the C191A mutant showed little or no oligomerization (Fig. 1f). Thus, GSDMD-NT palmitoylation is required for its oligomerization.

To quantify Cys191 palmitoylation, we used hydrogenation to release palmitate as ethyl palmitate (EP) from recombinant GSDMD expressed in mammalian cells under high-ROS conditions (see below), and detected it using mass spectrometry (MS)[21] with synthetic EP as a standard (Fig. 1g). EP was released from WT GSDMD at 91%, but not from GSDMD(C191A) (Fig. 1h and Extended Data Fig. 2a). We also used intact native MS and, despite the expected lability of palmitoylation[22], detected the existence of a peak +238 Da (palmitate) heavier in recombinant GSDMD-NT, the identity of which was confirmed by top-down sequencing (Supplementary Fig. 1e–h).

We next examined whether palmitoylated GSDMD exhibited increased in vitro liposomal release of pre-encapsulated Tb^{3+} dye. Several forms of mammalian and *Escherichia coli*-expressed full-length GSDMD were mixed with liposomes and cleaved by CASP1 to generate GSDMD-NT to initiate pore formation. All of the samples showed equal GSDM cleavage (Extended Data Fig. 2b). Notably, mammalian GSDMD induced faster liposome leakage compared with all of the other GSDMD forms at the same concentrations—over tenfold faster in the initial rate—and C191A or depalmitoylation by HA treatment markedly reduced liposome leakage (Fig. 1i). H_2O_2-treated, oxidized bacterial GSDMD did not enhance liposome leakage, suggesting that the previously noted role of ROS in enhancing GSDMD pore formation[23,24] was not due to direct oxidation. Notably, bacterially expressed human GSDMD was also palmitoylated at a low level, probably by autopalmitoylation[25], and not restricted to Cys191 (Extended Data Fig. 2c). Palmitoylation also enhanced liposome association of GSDMD-NT in a pelleting experiment (Extended Data Fig. 2d).

GSDMD palmitoylation during inflammasome activation

To investigate whether GSDMD is palmitoylated during inflammasome activation, we performed ABE analysis of THP-1 cells, a human monocytic cell line that endogenously expresses inflammasome pathway proteins. GSDMD palmitoylation was not detected after HA treatment alone. Lipopolysaccharide (LPS) priming or nigericin alone increased palmitoylated GSDMD but did not cause GSDMD processing; LPS plus nigericin, which activates the NLRP3 inflammasome, increased both GSDMD palmitoylation and cleavage (Extended Data Fig. 2e). When THP-1 cells were differentiated to macrophage-like cells by pretreatment with phorbol-12-myristate-13-acetate (PMA), nigericin alone and LPS plus nigericin both induced GSDMD cleavage and palmitoylation, and 2-BP significantly blocked palmitoylation (Fig. 2a and Extended Data Fig. 2f). Activation of NLRP3 in THP-1 macrophages by nigericin alone is consistent with previous studies[26]. All subsequent experiments used PMA-differentiated THP-1 cells. Mouse immortalized bone-marrow-derived macrophages (iBMDMs) behaved similarly to THP-1 monocytes (Extended Data Fig. 2g). Thus, inflammasome activation is associated with elevated GSDMD palmitoylation in both mouse and human cells.

To examine the role of Cys191 of GSDMD, we reconstituted *GSDMD*-knockout (KO) THP-1 cells or mouse iBMDMs with WT, C191A or cleavage-deficient D275A GSDMD fused to GFP, at levels comparable to endogenous GSDMD (Extended Data Fig. 2h,i and Supplementary Fig. 2). In contrast to WT-GSDMD-reconstituted THP-1 cells and iBMDM clones, LPS plus nigericin treatment of those reconstituted with C191A did not induce

GSDMD palmitoylation, pyroptosis, IL-1β release or significant membrane staining (Fig. 2b–k and Extended Data Fig. 2j). Notably, uncleavable GSDMD(D275A) also induced significant cell death and IL-1β release (see more below) (Fig. 2c–e,i and Extended Data Fig. 2j).

GSDMD palmitoylation is enhanced by ROS

As ROS enhances GSDMD pore formation[23,24], we tested whether ROS could enhance palmitoylation. We used the mitochondrial complex I inhibitor rotenone (ROT) and complex III inhibitor antimycin A (AMA) to increase ROS production[27] and the ROS scavengers *N*-acetylcysteine (NAC) and Tiron, and the mitochondrial ROS scavenger MitoTEMPO (MitoT) to reduce ROS. In HEK293T cells expressing GSDMD-NT, 35% of GSDMD-NT was palmitoylated, but ROT and AMA significantly increased (79.1% and 85.2%), NAC, Tiron and MitoT significantly decreased (4–11%), and 2-BP nearly abolished (0.6–1.7%) GSDMD-NT palmitoylation (Fig. 3a and Extended Data Fig. 3a). Using APE to visualize modified and unmodified GSDMD-NT on the same gel gave similar estimates for the extent of palmitoylation (Fig. 3b and Extended Data Fig. 3b). Cell death and GSDMD-NT membrane localization were increased in ROT- or AMA-treated cells but reduced after ROS scavenger or 2-BP treatment (Fig. 3c,d, Extended Data Fig. 3c–e and Supplementary Fig. 1i). The degree of GSDMD-NT palmitoylation and PI positivity was strongly correlated (R^2 = 0.94; Extended Data Fig. 3f).

We next examined the effect of ROS on palmitoylation in THP-1 cells activated by LPS plus nigericin, and pretreated or not with ROS generators or quenchers. Compared with LPS plus nigericin alone, ROT or AMA significantly increased GSDMD palmitoylation, whereas NAC, Tiron and MitoT decreased, GSDMD palmitoylation (Fig. 3e,f). The western blots showed total GSDMD from both cells and their debris in culture supernatants. Neither 2-BP nor ROS modulators altered GSDMD processing, in agreement with a recent study[28]. ROS levels measured by MitoSOX or CellROX, palmitoylation by APE, cell death by PI staining and LDH release, and IL-1β by ELISA changed in parallel, with ROT or AMA treatment increasing, and NAC, Tiron and MitoT decreasing all of these metrics (Fig. 3g,h and Extended Data Fig. 3g–k), supporting that ROS modulate GSDMD palmitoylation. In *GSDMD*-KO THP-1 cells reconstituted with GSDMD–GFP, GSDMD–GFP membrane staining increased after LPS and nigericin and was further enhanced by ROS activators and reduced by ROS scavengers (Fig. 3i, Extended Data Fig. 3l, Supplementary Figs. 3 and 4 and Supplementary Videos 1 and 2). The suppressive effect of ROS quenchers was almost equivalent to the 2-BP palmitoylation inhibitor, suggesting the close coupling between ROS and palmitoylation and the requirement of palmitoylation for GSDMD pore formation and cell death.

Previously, Dox-induced mouse GSDMD-NT in iBMDMs appeared to exhibit up to 22.9% oxidation at Cys192 by MS[23]. However, the MS approach used was unable to detect TCEP-resistant covalent modifications, including palmitoylation, and would therefore overestimate cysteine oxidation. Analysis of GSDMD cysteine oxidation in inflammasome-activated THP-1 cells by pulling-down oxidized cysteine (sulfenic acid) residues[23,29] showed only 5% and 3.2% oxidized full-length GSDMD and GSDMD-NT, respectively, even with ROS

activators (Extended Data Fig. 4a). Chemically, GSDMD oxidation and palmitoylation are not interconvertible. Thus, GSDMD oxidation constitutes a small alternative competing pathway, different from the tightly regulated palmitoylation of GSDMD.

ROS inducers were previously shown to lead to IL-1β secretion[27], but this result could not be replicated by others[30]. For clarification, we tested different doses and treatment duration of ROT (5–80 μM) and AMA (5–80 μg ml^{-1}) in differentiated and LPS-primed THP-1 cells. Treatment with 10 μM ROT or 10 μg ml^{-1} AMA for a maximum of 4 h, as used throughout the current study, did not lead to GSDMD or pro-IL-1β processing (Supplementary Fig. 5a,b). Only much higher concentrations and longer incubations caused GSDMD or pro-IL-1β processing. Furthermore, we performed unbiased RNA-sequencing (RNA-seq) analysis in THP-1 cells, showing large transcriptional differences between untreated and LPS plus nigericin treatment, but little difference among the LPS plus nigericin groups with or without 2-BP or NAC (Supplementary Fig. 5c–e), supporting a role of ROS or palmitoylation in post-transcriptional, rather than transcriptional, changes during inflammasome activation.

Canonical/non-canonical inflammasome activators

We determined whether ROS-dependent GSDMD palmitoylation is induced downstream of other inflammasomes. LPS plus monosodium urate, ATP or dsDNA electroporation to activate the NLRP3 and AIM2 canonical inflammasomes, and LPS electroporation to activate the non-canonical inflammasome in THP-1 cells, or bacterial flagellin (flatox) to activate the NAIP5–NLRC4 canonical inflammasome in mouse iBMDMs[31], all increased full-length GSDMD and GSDMD-NT palmitoylation, cell death and cellular and mitochondrial ROS, which were further enhanced by ROS activators and suppressed by ROS quenchers (Fig. 3j and Supplementary Figs. 6 and 7). Thus, both canonical and non-canonical inflammasome activation induces ROS-regulated GSDMD palmitoylation, which is required for cell death. ROS manipulations did not affect GSDMD cleavage induced by any of the inflammasomes tested.

Palmitoylation reinforcement by a feedforward loop

In *GSDMD*-KO THP-1 cells stimulated with LPS plus nigericin, ROS was not induced unless cells were rescued to express GSDMD or treated with ROS inducers such as AMA or ROT. Reconstitution with GSDMD(C191A) generated much less ROS in response to LPS plus nigericin compared with WT GSDMD (Extended Data Fig. 4b–g). Thus, ROS generation after LPS plus nigericin treatment is GSDMD dependent. Cleaved GSDMs are known to interact with the mitochondrial lipid cardiolipin[3,4,7,8] to form pores that damage mitochondria and generate ROS[32], and we revealed that only palmitoylated GSDMD was recruited to mitochondria after inflammasome stimulation (Extended Data Fig. 4h,i). Cardiolipin is synthesized by cardiolipin synthase 1 (encoded by *Crls1*)[33] and mainly localizes at the matrix side of the inner mitochondrial membrane[34–37] but can be translocated by phospholipid scramblase-3 (*Plscr3*)[38] to the outer mitochondrial membrane where it is accessible to cytosolic GSDMs. GSDMD association with mitochondria and ROS generation were barely detectable in *Crls1*- or *Plscr3*-KO iBMDMs (Extended Data Fig.

4j–l), as also shown previously[32]. Thus, the main source of ROS during inflammasome activation is mitochondrial, and generated by palmitoylated GSDMD. These findings suggest a feedforward loop in which palmitoylated GSDMD leads to mitochondrial ROS production, and ROS production leads to enhanced GSDMD palmitoylation.

Intact GSDMD forms pores similar to GSDMD-NT

LPS plus nigericin treatment of *GSDMD*-KO human or mouse cells rescued with cleavage-deficient GSDMD(D275A) induced low, but significant, amounts of ROS, cell death and IL-1β release, suggesting that uncleaved GSDMD may also form pores (Fig. 2c–e,i and Extended Data Fig. 2j). Indeed, liposome leakage by recombinant, palmitoylated WT and D275A GSDMD was significant, although reduced relative to palmitoylated GSDMD-NT (Fig. 4a). Bacterially expressed WT GSDMD or mammalian expressed C191A or C191A/D275A mutants barely induced liposome leakage above the background (Fig. 4a). Negative-stain EM analysis of GSDMD(D275A) reconstituted with liposomes, either before or after detergent solubilization, revealed approximately 30-nm-diameter pore-like structures, similar to GSDMD-NT pores[8] (Extended Data Fig. 5a,b). Thus, full-length GSDMD can form pores, but only if palmitoylated.

We next determined the cryo-EM structure of the palmitoylated GSDMD(D275A) pore at 5.5 Å resolution (Extended Data Fig. 5c,d and Supplementary Table 1), revealing a 33-fold symmetric GSDMD pore that is similar to the GSDMD-NT pore[8] but with prominent extra densities (Fig. 4b and Extended Data Fig. 5e). The density situated next to the NT probably corresponds to GSDMD-CT (Fig. 4b), which may be flexibly linked to GSDMD-NT. Another density extends from the end of the inserted β-barrel where Cys191 localizes (Fig. 4c), and probably corresponds to the flexibly attached palmitate group (Fig. 4b). The β-barrel density fits well with the previous GSDMD-NT pore structure; however, the globular rim fits only with that observed previously in the GSDMD-NT pre-pore[8], suggesting a flexibly linked rim to the β-barrel (Fig. 4c and Extended Data Fig. 5f,g). In the structure, GSDMD-CT localizes on the same plane as the transmembrane region. We anticipate that, in the presence of a membrane, GSDMD-CT and the associated GSDMD-NT rim could assume a different conformation, to not clash with the membrane. We also determined the cryo-EM structure of palmitoylated, monomeric WT GSDMD, and found that the fitted NT and CT domains[12] in our model have less contact, which suggests that palmitoylation should help to overcome autoinhibition (Extended Data Fig. 5h–j and Supplementary Table 2).

GSDMD induces cell death only when palmitoylated

The functional role of intact GSDMD was first validated by expressing the D275A uncleavable mutant in HEK293T cells, showing its palmitoylation, cell death and ROS induction, and membrane localization (Supplementary Fig. 8). Despite being significantly higher than GSDMD(C191A) (~2–6%), cell death by WT and D275A GSDMD (~10–15%) was relatively low, which may explain why pore formation by intact GSDMD was not noted before[2,4]. ROS activators further enhanced palmitoylation, and approximately doubled cell death and the proportion of cells with GSDMD membrane staining of intact GSDMD(D275A), but not GSDMD(C191A) or GSDMD(D275A/C191A).

Cell death was also induced at a low level by ROS activators in WT THP-1 cells or *GSDMD*-KO THP-1 cells that were reconstituted with GSDMD(D275A), but not in *GSDMD*-KO THP-1 cells, which was associated with increased GSDMD palmitoylation that was less prominent than that by inflammasome activation (Fig. 4d and Extended Data Fig. 6a–d). While ROT or AMA induced ROS independent of GSDMD (Extended Data Fig. 6e), ROS-mediated cell death was GSDMD dependent. Similarly, only when reconstituted with GSDMD(D275A), *GSDMD*-KO THP-1 cells exhibited enhanced palmitoylation, cell death, IL-1β release, ROS and cell surface GSDMD localization after LPS and nigericin treatment with or without ROS activators (Fig. 4e–i and Extended Data Fig. 6f–j). In two *Gsdmd*-KO iBMDM clones reconstituted to express an endogenous level of GSDMD(D275A)–GFP, GSDMD was palmitoylated in a ROS-dependent manner, and LPS plus nigericin induced pyroptosis in the absence of GSDMD cleavage (Extended Data Fig. 7 and Supplementary Fig. 9), confirming that uncleaved GSDMD forms pores in both human and mouse cells.

GSDMD(V41A) increases palmitoylation and cell death

A recent genetic analysis of de novo and inherited variants in a large cohort of individuals with autism identified a potential association between autism and the GSDMD(V41A) mutation[39]. Val41 localizes at the GSDMD NT–CT interface (Fig. 4j). Thus, the mutation could weaken autoinhibition to increase spontaneous GSDMD activity. Expression of full-length GSDMD(V41A) in HEK293T cells increased spontaneous GSDMD palmitoylation and cell death compared to WT GSDMD, which were enhanced by AMA and suppressed by NAC (Fig. 4k,l). These data suggest that palmitoylation is required for GSDMD(V41A) activation and suggest a possible pathophysiological role for inflammasome- and cleavage-independent GSDMD activation.

BMDM ROS- and GSDMD-dependent palmitoylation

To examine whether conclusions from cell lines held true for primary cells, we used WT, *Gsdmd*-KO and *Casp1/11*-double-KO (dKO) primary mouse BMDMs. Treatment of LPS plus nigericin induced GSDMD palmitoylation and cell death in WT but not *Gsdmd*-KO BMDMs, and the palmitoylation and cell death were further modulated by ROS activators and quenchers (Extended Data Fig. 8a,b and Supplementary Fig. 10a). GSDMD-cleavage-independent pore formation and cell death was shown using *Casp1/11*-dKO BMDMs after treatment by LPS plus nigericin with or without ROS modulators (Extended Data Fig. 8c–f and Supplementary Fig. 10b).

To monitor cell death by ROS-induced intact GSDMD activation, we followed PI staining using live-cell analysis using the IncuCyte system[40] on *Casp1/11*-dKO and *Gsdmd*-KO primary BMDMs. The lower dose of 10 μg ml^{-1} AMA or 10 μM ROT induced around 20% PI positivity in *Casp1/11*-dKO BMDMs, but none in *Gsdmd*-KO BMDMs, with no difference in the levels of annexin V staining (Extended Data Fig. 8g,h and Supplementary Fig. 10c). When the doses were raised to 30, 50 and 80 μg ml^{-1} AMA or 30, 50 and 80 μM ROT, the percentage of PI positivity remained significantly higher in *Casp1/11*-dKO BMDMs compared with in *Gsdmd*-KO BMDMs (Extended Data Fig. 8g and Supplementary

Fig. 10c). WT primary BMDMs exhibited similar ROS-dependent cell death that was entirely and partly dependent on GSDMD, respectively, at lower and higher ROT or AMA doses (Extended Data Fig. 8i and Supplementary Fig. 10d). Moreover, in primary *Casp1/11*-dKO but not *Gsdmd*-KO BMDMs, intact GSDMD palmitoylation and cell death were induced by dsDNA electroporation, flatox treatment and LPS electroporation, which were enhanced by ROT and suppressed by 2-BP and NAC (Extended Data Fig. 9). Thus, data in primary cells further demonstrated intact GSDMD palmitoylation and cell death induction.

GSDMD is palmitoylated mainly by ZDHHC5 and ZDHHC9

The thioesterification of palmitate to Cys residues on target proteins is catalysed by Asp-His-His-Cys (ZDHHC)-family palmitoyl *S*-acyltransferases (PATs) with 23 members in humans (ZDHHC1–9 and 11–24)[41]. To elucidate which ZDHHCs palmitoylate GSDMD, we co-expressed all 23 ZDHHCs with GSDMD in HEK293T cells and performed click chemistry detected by rhodamine fluorescence (Supplementary Fig. 11a). Probably because GSDMD was already significantly palmitoylated when transfected alone, co-expression with ZDHHCs had relatively modest effects on GSDMD palmitoylation. Nonetheless, ZDHHC1, 5, 9, 12, 17 and 19–21 appeared to increase GSDMD palmitoylation (Supplementary Fig. 11a).

As only ZDHHC5, 9, 12, 17 and 20 are significantly expressed in THP-1 and HEK293T cells (Supplementary Fig. 11b), we used siRNAs to knockdown these five ZDHHCs. In HEK293T cells transfected with GSDMD-NT, siRNAs against *ZDHHC5* and, to a lesser extent, *ZDHHC*9—but not *ZDHHC12*, *ZDHHC17* and *ZDHHC20*, scrambled siRNA (scRNA) or pooled siRNAs of all human ZDHHCs except for *ZDHHC5* and *ZDHHC9*—affected GSDMD-NT palmitoylation (Fig. 5a,b and Extended Data Fig. 10a). Most human ZDHHCs have been shown to localize to the early biosynthetic pathway (endoplasmic reticulum and Golgi), but ZDHHC5 is also localized to the plasma membrane[42–45]. Fluorescence imaging of co-expressed ZDHHC5–YFP and ZDHHC9–YFP with GSDMD–mCherry confirmed their co-localization, and co-immunoprecipitation of ZDHHS5 and ZDHHS9 (catalytic mutants of ZDHHCs) by GSDMD–Flag validated the interactions (Fig. 5c and Extended Data Fig. 10b,c). Knockdown of *ZDHHC5*, *ZDHHC9* or both by siRNA decreased PI positivity and LDH release, increased cell viability and impaired membrane localization (Fig. 5d,e and Extended Data Fig. 10d–f).

In THP-1 cells, siRNA knockdown of *ZDHHC5*, *ZDHHC9* or both, but not pooled siRNAs of all human ZDHHCs except for *ZDHHC5* and *ZDHHC9*, followed by LPS plus nigericin stimulation decreased palmitoylation of GSDMD-NT and full-length GSDMD without affecting GSDMD cleavage, reduced cell death, decreased IL-1β release and compromised GSDMD localization to the cell surface membrane (Fig. 5f–h, Extended Data Fig. 10g–m and Supplementary Fig. 11c). We also used CRISPR–Cas9 to knockout *ZDHHC5*, *ZDHHC9* or both in THP-1 cells, and showed that single ZDHHC deficiency reduced and double ZDHHC deficiency abolished LPS and nigericin-induced GSDMD palmitoylation and cell death (Fig. 5i,j and Extended Data Fig. 10n–p). By contrast, inhibition of depalmitoylation by palmostatin B, which inhibits the acyl protein thioesterase 1 (APT1), or ML348 and ML349, which inhibit APT1 and APT2, respectively, minimally altered GSDMD

palmitoylation induced by LPS plus nigericin and AMA in *GSDMD*-KO THP-1 cells reconstituted with GSDMD(D275A)–GFP, but strongly elevated GSDMD palmitoylation in cells treated with LPS plus nigericin and NAC (Fig. 5k). These data together illustrate the intricate regulation of *S*-palmitoylation by both palmitoyltransferases and depalmitoylases.

ROS reduces proteasomal degradation of ZDHHCs

We examined the expression of palmitoyltransferases and depalmitoylases. After treatment of THP-1 cells with LPS and nigericin, the levels of ZDHHC5 and ZDHHC9 were upregulated, further enhanced by ROS activators and suppressed by NAC, at up to 6.3-fold (Fig. 5l). This upregulation is consistent with the strong inhibitory effects on GSDMD palmitoylation by 2-BP under all of the conditions tested. By contrast, the levels of ZDHHC3 or depalmitoylases APT1 and APT2 were not grossly altered (Fig. 5l), supporting that ROS-associated GSDMD palmitoylation might be mainly due to upregulation of ZDHHC5 and ZDHHC9.

We next tested the hypothesis that decreased proteasomal degradation might be the reason for ZDHHC upregulation. We treated THP-1 cells with the proteasome inhibitor bortezomib (BTZ) or the protein synthesis inhibitor cycloheximide (CHX) on top of inflammasome activation and ROS modulation. We found that BTZ upregulated ZDHHC5 to similar levels in all conditions, suggesting that protein degradation is a main regulatory mechanism for ZDHHC5 (Fig. 5m). ROT-treated THP-1 cells with or without BTZ showed similar ZDHHC5 levels, suggesting that proteasomal activity on ZDHHC5 was nearly abolished by ROT. The ZDHHC5 level decreased to a low basal level after CHX treatment together with DMSO or LPS, but still increased when CHX treatment was coupled with LPS and nigericin or with additional ROT, again pointing to a proteasome-dependent mechanism (Fig. 5m). How ROS or inflammasome activation modulates proteasomal degradation of ZDHHC5 remains unclear and would be a good question to examine in subsequent studies.

Discussion

Our data provide the following model for how ROS and palmitoylation activate GSDMD pore formation (Fig. 5n). GSDMD palmitoylation is absent and slightly elevated in the resting state and after priming, respectively. After stimulation of inflammasome activation, palmitoylated GSDMD-NT (the most active form of GSDMD), although initially at a low level, and possibly palmitoylated full-length GSDMD, damages the mitochondria[32] to elevate ROS generation. Higher ROS in turn upregulates ZDHHC5 and ZDHHC9, leading to more GSDMD palmitoylation. This feedforward loop naturally leads to high ROS and robust GSDMD activation by palmitoylation, which can be further enhanced by exogenous ROS activators. In our experiments, GSDMD palmitoylation and activation in the absence of inflammasome activation requires exogenous ROS activators. However, any pathophysiological stress with ROS generation could result in enhanced palmitoylation of GSDMD to induce pyroptosis independent of inflammasomes. The fact that palmitoylation appears to be a common modification of the GSDM family may further implicate pyroptosis as a crucial downstream cellular consequence of high ROS.

The specific effect of reversible and regulated palmitoylation downstream of the rather non-specific ROS stands in contrast to ROS-induced oxidation[23,24] as a minor alternative pathway irrelevant to GSDMD pore formation and unregulated autopalmitoylation of bacterial GSDMs[25]. By contrast, multiple small molecules and endogenous fumarate target Cys191 to inhibit GSDMD functions in cells[46–48], probably at least in part by competition with GSDMD palmitoylation. We further speculate that the membrane-inserted lipid acyl chains at the GSDMD-NT pore may cause phase separation of surrounding lipids to induce GSDMD pore clustering, like the effect by *S*-palmitoylated SARS-CoV-2 spike protein[49]. More studies are required to deepen our understanding on the ROS–palmitoylation axis established in our study.

Online content

Any methods, additional references, Nature Portfolio reporting summaries, source data, extended data, supplementary information, acknowledgements, peer review information; details of author contributions and competing interests; and statements of data and code availability are available at https://doi.org/10.1038/s41586-024-07373-5.

Methods

Cell lines

Human monocytic THP-1 and HEK293T cell lines were purchased from ATCC. *GSDMD*-KO THP-1 cells were a gift from D. Bachovchin[51]. WT and *GSDMD*-KO iBMDMs cells were obtained as described previously[23,24]. *Crls1*-KO iBMDMs and *Plscr3*-KO iBMDMs were obtained as described[32].

Generation of primary BMDMs

BMDMs were generated from bone marrow extracted from healthy adult (aged >8 weeks) male or female WT C57BL/6J, *Gsdmd*-KO and Casp1/11-dKO mice according to previously published protocols[52] with minor modifications. Mice were euthanized and hind leg bones (femurs + tibias) were removed, cleaned of muscle and connective tissue and placed in complete DMEM for short-term storage. Under sterile conditions, tips of bones were cut and two bones each were placed in a sterile 0.65 ml microcentrifuge tube, of which the bottom was perforated using a syringe needle and placed in a sterile 2 ml tube. Bone marrow was spun out of bones in a microcentrifuge for 30 s to 1 min at 8,000*g* and collected in 2 ml tube. Bones and other tissue left in 0.65 ml tubes were discarded and bone marrow was resuspended in 1 ml of ACK lysing buffer and incubated for 3 min at room temperature to lyse red blood cells. ACK buffer was quenched with 5 ml of complete DMEM and the cell suspension was passed through a 70 μm cell strainer into a 50 ml tube. Cells were washed once with 10 ml of complete DMEM and the cell number was determined. If applicable, bone marrow cells were cryopreserved in FCS + 10% DMSO and stored at −80 °C or in liquid nitrogen storage for later use. In total, 4–5 × 10^6 bone marrow cells (fresh or cryopreserved) per plate were seeded in non-TC treated 10 cm plates in 10 ml of complete DMEM supplemented 30% of L929 supernatants containing M-CSF. The medium

was replenished with 5 ml of fresh complete DMEM + 30 % L929 supernatants after 3 days and cells were used for experiments after 6–8 days of differentiation.

Constructs

Full-length human GSDMD containing an internal human rhinovirus 3C protease (3C) site was cloned into the pDB.His.MBP vector after the N-terminal His6-maltose-binding protein (MBP) tag as previously described (GSDMD-MBP-3C)[8] and the C191A mutant was generated. Full-length human GSDMD was cloned into the pDB.His. SUMO vector using the Gibson Assembly Master Mix (New England Biolabs, E2611L) and the C191A mutant was generated. GSDMD-FL, GSDMD-NT and GSDMD-CT were amplified by PCR and subcloned into a pLV vector containing C-terminal mCherry (GSDMD-mCherry) or the pcDNA3.1 vector tagged with C-terminal Flag (GSDMD-Flag). Full-length GSDMA and GSDMB were cloned into the pCMV4 vector with N-terminal Flag. GSDMA-NT, GSDMA-CT, GSDMB-NT, GSDMB-CT, GSDMC-FL, GSDME-FL, GSDME-NT and GSDMD-CT were cloned into the pcDNA3.1 with C-terminal Flag. All plasmids were transformed into DH5α-competent cells (NEB, C2987U), subsequently mini-prepped (Qiagen) and verified by sequencing. HeaTil screen (human ZDHHC screen) plasmids pLH1–24 have been previously previously[41]. The CASP1 construct that co-expresses p20 and p10 subunits was a gift from T. S. Xiao[53]. For reconstitution of stable cell lines, GSDMD-NT (1–258 residues) tagged with GFP, and GSDMD-CT (259–484 residues) were amplified by PCR and subcloned into a pLVX vector to make internal GFP-tagged GSDMD constructs using the Gibson Assembly Master Mix (New England Biolabs, E2611L). Active and inactive flatox constructs were ordered from Addgene (active flatox, 84871; inactive flatox, 84872). All mutations in this study were introduced using the QuikChange II XL site-directed mutagenesis kit (Agilent Technologies, 200521), KLD Enzyme Mix (New England Biolabs, M0554S) or Gibson Assembly Master Mix (New England Biolabs, E2611L).

Mammalian cell culture and transfection

HEK293T cells and iBMDMs were cultured in Dulbecco's modified Eagle's medium with glutamine (DMEM, Gibco, Thermo Fisher Scientific) supplemented with 10% fetal bovine serum (FBS, Sigma-Aldrich, TMS-013-B), 1% penicillin–streptomycin mix (Gibco, Thermo Fisher Scientific), l-glutamine (Gibco, Thermo Fisher Scientific) and sodium pyruvate (Gibco, Thermo Fisher Scientific). THP-1 cells were maintained in Roswell Park Memorial Institute medium (RPMI1640, Gibco, Thermo Fisher Scientific) with l-glutamine, supplemented with 10% FBS and 1% penicillin–streptomycin mix (Gibco, Thermo Fisher Scientific), and were differentiated by treatment with 200 ng ml^{-1} PMA (Sigma-Aldrich, P8139–5MG) for 48 h. All cells were propagated in a humidified incubator at 37 °C and with 5% CO_2.

Expression and purification of GSDMD proteins in bacteria and Expi293 cells

GSDMD-MBP-3C WT and C191A mutant constructs were transformed into *E. coli* BL21 (DE3) cells (Agilent Technologies, 230280), plated and incubated overnight at 37 °C. Single colonies were picked the next day and grown in Luria broth (LB) medium supplemented with 50 μg ml^{-1} kanamycin at 37 °C. The cultures were induced at an optical density of 0.6 at 600 nm (OD_{600}) by 1 mM isopropyl β-d-1-thiogalactopyranoside and incubated for

18 h at 18 °C before collection. Cells were pelleted by centrifugation at 4,000*g* for 30 min and resuspended in buffer A (40 mM HEPES at pH 7.0, 150 mM NaCl) supplemented with 5 mM imidazole for lysis by sonication. His6-MBP-tagged GSDMD was enriched on Ni-NTA beads and eluted by buffer A supplemented with 500 mM imidazole. The His6-MBP tag was cleaved by His6-tagged tobacco etch virus (TEV) protease at 4 °C overnight. His6–MBP and His6–TEV were removed using a Ni-NTA column and the flow-through containing GSDMD was further purified using a Superdex 200 Increase 10/300 GL (Cytiva) size-exclusion column equilibrated with buffer A. Peak fractions were collected, analysed using SDS–PAGE for purity and snap-frozen for liposome leakage assays.

The GSDMD-Flag WT or indicated mutant constructs were transfected into Expi293 cells that were maintained in 1,000 ml Expi293 expression medium (Thermo Fisher Scientific), fed with 6 mM KCl and grown to 2.5×10^6 cells per ml, using polyethylenimine (PEI, Polysciences). The cells were fed with 10 mM sodium butyrate and 10 ml 45% d-(+)-glucose solution 12 h after transfection. The cells were grown for another 2 days and collected by centrifugation at 4,000*g* for 30 min. The cell pellet was resuspended in buffer A and lysed by sonication (2 s on, 8 s off, 3.5 min total on, 40% power), and centrifuged at 40,000 rpm for 1 h. The supernatant was collected and incubated with anti-Flag M2 Affinity Gel (Sigma-Aldrich, A2220–4X25ML) overnight at 4 °C with gentle rotation. After washing, the protein was eluted using buffer A with 150 ng μl^{-1} 3× Flag peptide (Sigma-Aldrich, F4799–25MG). The eluted GSDMD protein was snap-frozen for other assays. To obtain highly palmitoylated GSDMD, AMA (Sigma-Aldrich, A8674) at 10 μg ml^{-1}, or ROT (Sigma-Aldrich, R8875–1G) at 10 μM was used to treat Expi293 cells for 4 h before collection.

ABE

ABE was performed according to a previously described procedure with modifications[54]. Cells were treated and collected as specified and centrifuged. Cell pellets were resuspended in 0.2 ml buffer A (50 mM Tris-HCl pH 7.4, 1 mM EDTA, 150 mM NaCl, 1% NP-40) with 20 mM *N*-ethylmaleimide (NEM, Sigma-Aldrich, E3876–5G) and protease inhibitor cocktail. The samples were incubated for 2 h with gentle rotation at 4 °C and centrifuged at 20,000*g* for 20 min. The supernatant was collected and the Pierce BCA Protein Assay Kit (Thermo Fisher Scientific, 23225) was used to determine the protein concentration to equalize the amount of protein in each sample.

The sample was then precipitated with a methanol–chloroform–water mixture. In brief, 800 μl methanol, 300 μl chloroform and 600 μl double-distilled H_2O were added to each sample sequentially with thorough mixing by vortexing at each step. The mixtures were centrifuged for 5 min at 16,000*g* in a microfuge and the top aqueous layer was discarded. Then, 800 μl methanol was added to resuspend each pellet. The mixtures were thoroughly vortexed and centrifuged for 5 min at 16,000*g*, and the supernatants were removed as much as possible. The pellets were air-dried for 15–20 min. The above methanol–chloroform precipitation was repeated two additional times.

The dried pellets were resuspended in 0.2 ml buffer B (50 mM Tris-HCl pH 7.4, 5 mM EDTA, 150 mM NaCl, 1% NP-40, 1% SDS) with or without 0.7 M HA (50%

by weight in H_2O, Sigma-Aldrich, 438227–50ML) to totally dissolve the pellets by pipetting or even water sonication and incubated with gentle rotation at room temperature for 1 h. The samples were precipitated using the same above methanol–chloroform protocol and dissolved in buffer B with 4 mM *N*-[6-(biotinamido)hexyl]-3′-(2′-pyridyl dithio)propionamide (biotin-HPDP, Cayman Chemical Company, 16459) and incubated with gentle rotation at room temperature. After incubation for 1 h, the samples were precipitated by the same above methanol–chloroform protocol three times.

After drying, the pellets were resuspended in 0.1 ml buffer B, and a certain percentage of each sample was taken out as a loading control. The SDS concentration in each remaining sample was diluted tenfold to 0.1% by buffer C (50 mM Tris-HCl pH 7.4, 1 mM EDTA, 150 mM NaCl) before adding 30 µl prewashed Streptavidin agarose (Thermo Fisher Scientific, 29200). The mixture was incubated overnight at 4 °C with rotation. The agarose beads were washed three times using buffer C with 0.1% NP-40 and 0.1% SDS, mixed with 2× SDS-Laemmli buffer containing β-mercaptoethanol and incubated at 98 °C for 5 min before running an SDS–PAGE on Mini-PROTEAN TGX Precast Protein Gels (Bio-Rad). The gels were then transferred and immunoblotted with appropriate antibodies.

IncuCyte analysis

Cells were seeded in 96-well plates. After 24 h, cells were treated or not with AMA (Sigma-Aldrich, A8674) at 10 µg ml^{-1}, ROT (Sigma-Aldrich, R8875–1G) at 10 µM, *N*-acetyl cysteine (NAC, Sigma-Aldrich, A9165–25G) at 15 mM, Tiron (Bio Basic TB0951) at 5 mM or MitoTempo (MitoT, Sigma-Aldrich, SML0737) at 500 µM for 4 h. At 3.5 h after AMA, ROT, NAC, Tiron or MitoT treatment, 1 µg ml^{-1} PI (BD Bioscience, 556463) was added for 30 min. An IncuCyte S3 Live-Cell Analysis System (Sartorius) was used to determinate the PI positivity by average red object integrated intensity.

For primary BMDMs, differentiated primary BMDMs were seeded in 96-well plates. For the LPS/nigericin treatment groups, after plating for 16 h, cells were pretreated or not with 2-BP (50 µM) for 30 min, and treated with AMA (10 µg ml^{-1}), ROT (10 µM), NAC (15 mM), Tiron (5 mM) or MitoT (500 µM) for 4 h, LPS (1 µg ml^{-1}) for 3 h and nigericin (20 µM) for 1 h. An IncuCyte S3 Live-Cell Analysis System (Sartorius) was used to determinate the PI positivity by average red object integrated intensity.

For ROS-alone treatment groups, cells after plating 16 h were treated with indicated concentration of AMA or ROT for 3 h, 1 µg ml^{-1} PI (BD Bioscience, 556463) or IncuCyte Annexin V Red (Sartorius, 4641, concentration according to the manufacturer's instruction) was added. An IncuCyte S3 Live-Cell Analysis System (Sartorius) was used to determinate the PI or IncuCyte Annexin V Red positivity by average red object integrated intensity for 3 h. Triton X-100 (0.1%) was used as the positive control.

Oxidized GSDMD pull-down

A total of 10×10^6 THP-1 cells was seeded in tissue culture-treated 10 cm dishes, treated with PMA and incubated at 37 °C and 5% CO_2 for 2 days. As indicated, cells were treated with AMA (10 µg ml^{-1}) or ROT (10 µM), and LPS (1 µg ml^{-1}) was added 1 h later. Nigericin (20 µM) was added after another 2 h, and cells were collected 1 h later. Thus, the

total treatment times for AMA/ROT, LPS and nigericin were 4, 3 and 1 h, respectively. After the treatment, cells were lifted using PBS + 4 mM EDTA, washed once in cold PBS and then directly resuspended in lysis buffer (RIPA) containing protease inhibitors and 100 mM NEM to directly label cysteine-containing proteins at the time of lysis.

Determination of relative cysteine oxidation was performed as described previously[23]. In brief, after incubation on ice for 2 h, the lysates were clarified by centrifugation at 16,000*g* at 4 °C for 20 min. Protein concentrations were normalized using the BCA Assay (Pierce BCA Protein Assay Kits, 23227). The excess NEM was removed by filtration with Zeba spin columns with a 7 kDa cut-off (Thermo Fisher Scientific, 89882) and sulfenic acid residues were selectively reduced with 200 mM sodium arsenite. Newly released free thiols were labelled by adding 1 mM biotin–maleimide (Sigma-Aldrich, B1267–25MG). After incubation at 37 °C for 1 h, the excess biotin–maleimide was removed using Zeba spin desalting columns. The protein mixture was precleared by using Sepharose 6B beads (Millipore Sigma) at room temperature for 2 h on a rotator. To pull-down biotin-labelled proteins, the eluate was further incubated with NeutrAvidin agarose beads (Thermo Fisher Scientific) at 4 °C for overnight. NeutrAvidin agarose was washed extensively with wash buffer (50 mM Tris, pH 7.5, 600 mM NaCl, 1 mM EDTA, 0.5% NP-40) and cold PBS. The NeutrAvidin agarose resin was boiled in 4× SDS buffer to elute enriched proteins. Proteins were separated by SDS–PAGE on 4–20% gradient Mini-PROTEAN TGX Precast Protein Gels (Bio-Rad). The gels were then transferred and immunoblotted with GSDMD antibody.

Global RNA-seq

THP-1 cells were treated and collected as specified and centrifuged. Total RNA was isolated using the RNAeasy Mini Kit (Qiagen, 74104) according to the manufacturer's instruction, and sequencing was performed by Azenta Life Sciences. Total RNA samples were quantified using Qubit 2.0 Fluorometer (Life Technologies) and RNA integrity was checked using Agilent TapeStation 4200 (Agilent Technologies). RNA-seq libraries were prepared using the NEBNext Ultra II RNA Library Prep Kit for Illumina according to the manufacturer's instruction (NEB). In brief, mRNAs were initially enriched with Oligod(T) beads. Enriched mRNAs were fragmented for 15 min at 94 °C. First-strand and second-strand cDNAs were subsequently synthesized. cDNA fragments were end repaired and adenylated at 3′ ends, and universal adapters were ligated to cDNA fragments, followed by index addition and library enrichment by PCR with limited cycles. The sequencing library was validated on the Agilent TapeStation (Agilent Technologies), and quantified using Qubit 2.0 Fluorometer (Invitrogen) as well as by qPCR (KAPA Biosystems). The sequencing libraries were multiplexed and clustered onto a flowcell on the Illumina NovaSeq instrument according to the manufacturer's instruction. The samples were sequenced using a 2 × 150 bp paired end configuration. Image analysis and base calling were conducted using the NovaSeq Control Software (NCS). Raw sequencing data (.bcl files) generated from Illumina NovaSeq was converted into fastq files and de-multiplexed using Illumina bcl2fastq v.2.20 software.

After investigating the quality of the raw data, sequence reads were trimmed to remove possible adapter sequences and nucleotides with poor quality. The trimmed reads were

mapped to the Human reference genome (GRCh38) available on ENSEMBL using the STAR aligner v.2.5.2b. The STAR aligner is a splice aligner that detects splice junctions and incorporates them to help align the entire read sequences. BAM files were generated as a result of this step. After extraction of gene hit counts, the gene hit counts table was used for downstream differential expression analysis. Differentially expressed genes were determined using DESeq2[55]. The Wald test was used to generate *P* values and $\log_2$-transformed fold changes. Genes with adjusted $P < 0.05$ and absolute $\log_2$[fold change] > 1 were called as differentially expressed genes for each comparison.

APE

APE largely followed the procedure described previously[50]. Cells were treated and collected as specified and centrifuged. Cell pellets were resuspended in 150 μl buffer A (50 mM Tris-HCl pH 7.4, 1 mM EDTA, 150 mM NaCl, 1% NP-40) and protease inhibitor cocktail. Samples were incubated for 2 h with gentle rotation at 4 °C and centrifuged at 20,000*g* for 20 min. The supernatant was collected and Pierce BCA Protein Assay Kit (Thermo Fisher Scientific, 23225) was used to determine the protein concentration to equalize the amount of protein in each sample. Each 200 μg of total protein was aliquoted and the volume adjusted to 92.5 μl by adding buffer A.

The sample was then treated with neutralized 10 mM TCEP for 30 min at room temperature with nutating mixing. Reduced cysteine residues were capped with freshly prepared 25 mM NEM by incubating for 2 h at room temperature with mixing by nutation. The sample was then precipitated with methanol–chloroform–water mixture (4:1.5:3). In brief, 400 μl methanol, 150 μl chloroform and 300 μl double-distilled H_2O were added to each sample sequentially with thorough mixing by vortexing at each step. The mixtures were centrifuged for 5 min at 20,000*g* in a microfuge and the top aqueous layer was discarded. Then, 1,000 μl methanol was added to resuspend each pellet and the mixtures were centrifuged for 5 min at 20,000*g*, and the supernatants were removed as much as possible. In total, 800 μl methanol was added to resuspend each pellet and the mixtures were centrifuged for 5 min at 20,000*g*, and the supernatants were removed as much as possible. The pellets were air-dried for 5 min, and the protein pellets were resuspended in 100 μl in buffer B (50 mM triethanolamine pH 7.3, 150 mM NaCl and 4% SDS). The above methanol–chloroform-H_2O precipitation was repeated two additional times.

The dried pellets were resuspended in 60 μl buffer B containing 4 mM EDTA and split into two samples containing either 90 μl 0.75 M HA (50% by weight in H_2O, Sigma-Aldrich, 438227–50ML) or 90 μl buffer C (50 mM triethanolamine pH 7.3, 150 mM NaCl and 0.2% Triton X-100). The mixtures were thoroughly vortexed and incubated for 1 h at room temperature with mixing by nutation. The samples were precipitated by the same methanol–chloroform–H_2O precipitation protocol.

After drying, the pellets were resuspended in 40 μl buffer B containing 4 mM EDTA, and a certain percentage of each sample was taken out as a loading control. The samples were then diluted with 90 μl buffer C containing 2 mM mPEG-Mal (10 kDa) final and incubated for 2 h at room temperature with mixing on a nutator. A final methanol–chloroform–H_2O precipitation was performed, and the pellet was resuspended in 50 μl of 1× Laemmli buffer

containing β-mercaptoethanol and incubated at 98 °C for 5 min before running an SDS–PAGE on 4–20% gradient Mini-PROTEAN TGX Precast Protein Gels (Bio-Rad). The gels were then transferred and immunoblotted with appropriate antibodies. For every mPEG-Mal coupled to the protein, there is an observed mass shift corresponding to twice the mass of the tag used[50].

ZDHHC5- and *ZDHHC9*-KO THP-1 cell lines

Two sgRNAs for each gene were chosen for knockout vector construction: *ZDHHC5*, GAGACCGGGACATACTTGCT; AGAGTGTCGTAGCTCCCACT; and *ZDHHC9*, TTTGCCGGGCCATCATGACG; ATGGCCGCGTCATGATGGCC.

The sgRNAs were cloned into lentiCRISPRv2-puro for ZDHHC5 (Addgene, 52961) or lentiCRISPRv2-blast for ZDHHC9 (Addgene, 98293) according to the Zhang laboratory protocol[56]. Lentivirus was packaged in Lenti-X293T cells (TaKaRa, 632180). In brief, 1 day before transfection, 0.5×10^6 Lenti-X 293T cells were seeded in each well of a six-well plate. Lentiviral plasmids with *ZDHHC5* or *ZDHHC9* sgRNAs or sgControl (Addgene, 125836)[57] were mixed with psPAX2 (Addgene, 12260) and pMD.2G (Addgene, 12259) at a 5:3:2 ratio and a total of 1 μg plasmids was added to 100 μl Opti-MEM with 4 μl PEI (1 mg ml^{-1}) and incubated 10 min at room temperature before adding to each well. The lentivirus supernatant was collected 48 h after transfection, filtered with a 0.45 μm PES filter, aliquoted and stored at −80 °C for long-term storage. For transduction, 3×10^5 THP-1 cells were seeded in a 12-well plate and lentivirus was added to the cells together with 10 μg ml^{-1} polybrene. Spinfection was performed with centrifugation at 1,000*g* at 30 °C for 1 h. The medium was replaced with complete RPMI 1640 and cultured for 2 days before adding antibiotic for selection (2 μg ml^{-1} of puromycin for sgZDHHC5 and sgControl; 10 μg ml^{-1} of blasticidin S for sgZDHHC9). After selection for 1 week, single clones of knockout THP-1 cells were sorted into 96-well plates using the Sony SH800Z sorter and verified by sequencing genomic DNA and immunoblotting. For generating *ZDHHC5* and *ZDHHC9* double-knockout cells, *ZDHHC5*-knockout pooled THP-1 cells after puromycin selection were transduced with sgZDHHC9 lentivirus and selected with blasticidin S for another week and sorted into single colons for further validation.

Intact and top-down MS

For intact MS and top-down MS analysis, around 10 μg of fast-protein-liquid-chromatography-purified GSDMD-NT was acid denatured by addition of 2% (v/v) acetic acid, followed by buffer-exchange into 75 mM ammonium acetate (pH 3.0 at 4 °C) using ZebaSpin desalting columns (Pierce). The sample was diluted to around 10 μM using 75 mM ammonium acetate with 2% acetic acid (v/v). In total, around 2–3 μl of this solution was loaded into a gold-coated borosilicate capillary prepared in-house and positioned in front of the inlet of a Thermo Fisher Scientific Orbitrap UHMR mass spectrometer. An electrospray was generated by applying a 0.9–1.3 kV bias to the capillary with 0.1–0.5 mbar of backing pressure in the positive-ion mode. The instrument was set to ‘high m/z transmission’ and the detector was set to ‘low m/z detection’. The remaining instrument parameters were tuned for transmission of high-molecular-mass ions[58]. Typical settings were as follows: in-source trapping, −10 – −100 V; injection flatapole, 5 V; interflatapole

lens, 4 V; bent flatapole DC, 3 V; bent flatapole gradient, 30 V; noise threshold, 3. MS1 spectra were collected at a resolution setting of 7,500 (at m/z 200) with a bias of 10–30 V applied across the high-energy collisional dissociation (HCD) cell. Three charge states corresponding to a protein weighing 27,903 ± 1 Da were identified; detailed analysis of the satellite features revealed a peak series that corresponded to species with a molecular mass that was +238 Da heavier than the main charge state distribution, consistent with palmitoylation.

To carry out top-down MS/MS analysis on each proteoform, peaks corresponding to ions of interest were isolated using a 10 Th isolation window with the quadrupole mass filter and subjected to collisional activation using the HCD cell (180–220 V). MS2 spectra were collected at a resolution setting of 100,000 (at m/z 200) after averaging 999 scans. MS1 spectra were extracted as text files from QualBrowser (v.4.1), plotted in OriginPro (2021, v.9.8), and manually assigned. MS2 spectra were analysed using Prosite Native[59] and TDValidator[60] with a fragment ion tolerance of 10 ppm. All fragment ions were manually validated. The resulting sequence maps confirmed that both the 27,903 ± 1 Da and the +238 peaks corresponded to GSDMD-NT with N-terminal acetylation and C-terminal truncation. Note that *S*-palmitoyl bonds are labile and are often lost as neutral fragments during HCD[22].

Sample preparation for UPLC–MS/MS analysis

Palmitoyl group on GSDMD was released by hydrogenation as previously described[21]. In total, 75 μg Expi293-expressed, palmitoylated GSDMD WT and 75 μg C191A mutant protein were lyophilized in a 5 ml silicon-coated glass tube overnight. Each sample was resuspended by adding 500 μl of solution-I (formic acid/absolute ethanol (1:4)) and mixed by vortexing until the solution was clear. The sample was washed by adding 1 ml of solution-II (solution-I/pentane (4:10)), mixing by vortexing for 1 min and centrifuging at 1,500*g* for 5 min at 4 °C to separate the organic and aqueous phases. The upper (organic) layer was removed, and the wash was repeated two more times. The sample was transferred to a 5 ml silicon-coated glass flask to which 5 mg of platinum(iv) oxide (Sigma-Aldrich, 206032–250MG) was added, and the reaction was allowed to proceed for 2 h under a hydrogen atmosphere at 25 °C with continuous stirring. After the hydrogenation reaction, 400 μl double-distilled water and 0.5 ml pentane were added to the flask, followed by vortexing for 1 min and centrifuging at 1,500*g* for 5 min at 4 °C. The upper organic layer, which contains the released lipids, was transferred to a new silicon-coated glass tube. The extraction was repeated twice using the same volumes of pentane. The extracted lipid was collected, and pentane was dried with nitrogen. The lipid was redissolved in 50 μl methanol and was used for UPLC–MS/MS.

UPLC–MS/MS analysis

Identification of released palmitate (as EP) from WT and mutant GSDMD was performed using the Vanquish UHPLC system (Thermo Fisher Scientific) coupled to a Q Exactive Orbitrap mass spectrometer (Thermo Fisher Scientific). The YMC Accura Triart C8 column (2.1 mm × 100 mm × 3 μm, 200 μl min^{-1}) was used with the following LC gradient: 50% 2-propanol/10% acetonitrile/0.05% formic acid isocratic for 2 min, a linear increase to 85% 2-propanol/10% acetonitrile/0.05% formic acid over 3 min and hold for 7 min, then

back to the initial conditions over 0.1 min, and hold for 7.9 min at 40 °C. The positive-ion mode method was established with the following heated electrospray ionization parameters: spray voltage, 3.80 kV; sheath gas, 40 AU; auxiliary gas, 8 AU; capillary temperature, 350 °C; Aux gas heater temperature, 350 °C; S-lens RF level, 65.0 AU. MS spectra (R = 70,000 at m/z 200) were acquired from 250 to 450 m/z. For MS/MS acquisition, the top 3 data-dependent acquisition (R = 17,500 at m/z 200, isolation window: 1.0 m/z, mean collision energy, 20 AU) was applied. The extracted ion chromatograms (XICs) and MS/MS spectra were generated using Qual Browser (Thermo Fisher Scientific Xcalibur 4.4). MS/MS spectra of released palmitate from WT were directly compared with a MS/MS spectrum of the synthetic EP (Sigma-Aldrich).

Generation of stable cell lines

To generate stable macrophage cell lines, HEK293T cells were used to produce lentiviruses. HEK293T cells were plated onto 10 cm tissue culture dishes and cultured at 37 °C with 5% CO_2. Then, 10 μg of pLVX plasmid containing the GSDMD-GFP or GSDMD-mCherry gene, 12 μg of psPAX2 packaging plasmid and 4 μg of pMD2.G envelope plasmid (both plasmids were a gift from D. Trono, Addgene, 12260 and 12259, respectively) were mixed together and co-transfected into HEK293T using PEI (DNA:PEI = 1:3) when the confluency was 60%. Then, 20 h after transfection, the medium was removed, and the cells were replenished with 10 ml of fresh medium and incubated for 48 h. The supernatant containing the lentiviruses was filtered using a 0.45 μm PES filter and used to infect THP-1 cells or iBMDMs. For infection, *GSDMD*-KO THP-1 cells or iBMDMs were plated onto six-well plates, and 10 μg ml^{-1} polybrene (Santa Cruz Biotechnology, sc-134220) was added to the medium to increase the efficiency of infection. To generate cells with equal expression levels to the WT cells, different amounts of the viruses were added to different wells above. The cells were incubated with the viruses for 72 h and positive cells were selected by flow cytometry. Selected cells were cultured and checked for expression by western blot to keep the expression level of GSDMD similar to the WT cells. For iBMDMs, monoclonal cell populations were isolated by limited dilution. Monoclonal cells were cultured and checked for GSDMD expression by western blot to keep the expression level of GSDMD similar to WT.

Sequence of GSDMD–GFP:

MGSAFERVVRRVVQELDHGGEFIPVTSLQSSTGFQPYCLVVRKPSSSWFWKPRYKC
VNLSIKDILEPDAAEPDVQRGRSFHFYDAMDGQIQGSVELAAPGQAKIAGGAAVSDS
SSTSMNVYSLSVDPNTWQTLLHERHLRQPEHKVLQQLRSRGDNVYVVTEVLQTQK
EVEVTRTHKREGSGRFSLPGATCLQGEGQGHLSQKKTVTIPSGSTLAFRVAQLVIDSD
LDVLLFPDKKQRTFQPPATGHKRSTSEGAWPQGGGGSGGGGSGGGGSMVSKGEELF
TGVVPILVELDGDVNGHKFSVSGEGEGDATYGKLTLKFICTTGKLPVPWPTLVTLTY
GVQCFSRYPDHMKQHDFFKSAMPEGYVQERTIFFKDDGNYKTRAEVKFEGDTLVN
RIELKGIDFKEDGNILGHKLEYNYNSHNVYIMADKQKNGIKVNFKIRHNIEDGSVQL
ADHYQQNTPIGDGPVLLPDNHYLSTQSALSKDPNEKRDHMVLLEFVTAAGITLGMD
ELYKGGGGSGGGGSGGGGSLPSGLSMMRCLHNFLTDGVPAEGAFTEDFQGLRAEV
ETISKELELLDRELCQLLLEGLEGVLRDQLALRALEEALEQGQSLGPVEPLDGPAGA

VLECLVLSSGMLVPELAIPVVYLLGALTMLSETQHKLLAEALESQTLLGPLELVGSLL
EQSAPWQERSTMSLPPGLLGNSWGEGAPAWVLLDECGLELGEDTPHVCWEPQAQG
RMCALYASLALLSGLSQEPH*

Sequence of GSDMD–mCherry:

MGSAFERVVRRVVQELDHGGEFIPVTSLQSSTGFQPYCLVVRKPSSSWFWKPRYKC
VNLSIKDILEPDAAEPDVQRGRSFHFYDAMDGQIQGSVELAAPGQAKIAGGAAVSDS
SSTSMNVYSLSVDPNTWQTLLHERHLRQPEHKVLQQLRSRGDNVYVVTEVLQTQK
EVEVTRTHKREGSGRFSLPGATCLQGEGQGHLSQKKTVTIPSGSTLAFRVAQLVIDSD
LDVLLFPDKKQRTFQPPATGHKRSTSEGAWPQGGGGSGGGGSGGGGSMVSKGEED
NMAIIKEFMRFKVHMEGSVNGHEFEIEGEGEGRPYEGTQTAKLKVTKGGPLPFAWDI
LSPQFMYGSKAYVKHPADIPDYLKLSFPEGFKWERVMNFEDGGVVTVTQDSSLQDG
EFIYKVKLRGTNFPSDGPVMQKKTMGWEASSERMYPEDGALKGEIKQRLKLKDGG
HYDAEVKTTYKAKKPVQLPGAYNVNIKLDITSHNEDYTIVEQYERAEGRHSTGGMD
ELYKGGGGSGGGGSGGGGSLPSGLSMMRCLHNFLTDGVPAEGAFTEDFQGLRAEV
ETISKELELLDRELCQLLLEGLEGVLRDQLALRALEEALEQGQSLGPVEPLDGPAGA
VLECLVLSSGMLVPELAIPVVYLLGALTMLSETQHKLLAEALESQTLLGPLELVGSLL
EQSAPWQERSTMSLPPGLLGNSWGEGAPAWVLLDECGLELGEDTPHVCWEPQAQG
RMCALYASLALLSGLSQEPH*

Cell viability and microscopy-based cytotoxicity assays

LDH release was measured using LDH-Glo Cytotoxicity Assay kit (Promega, J2380) according to the manufacturer's instructions. Cell viability was assessed by measuring ATP levels using the CellTiter-Glo Luminescent Cell Viability Assay (Promega, G7570) according to the manufacturer's instructions. Luminescence was measured on the SYNERGY microplate reader (Biotek). For microscopy-based cytotoxicity analysis, cells were seeded in 24-well plates or CELLview Cell Culture Dish with four compartments) (USA Scientific, 5662–7870) in culture medium with 1 μg ml^{-1} PI (BD Bioscience, 556463) or 0.5 μM Sytox Green (Thermo Fisher Scientific, S7020) followed by calculating PI positivity or Sytox Green positivity on either an Inverted Nikon Ti2 fluorescence microscope with a ×40 objective (NA = 1.2) with a stage-top incubator to maintain 37 °C and 5% CO_2 or on a Leica TCS SP8 Laser Scanning Confocal (Leica) fluorescence microscope with an incubator to maintain 37 °C and 5% CO_2.

Detection of human IL-1β by ELISA

A sandwich enzyme-linked immunosorbent assay detection (ELISA) kit for human IL-1β (Invitrogen, 88–7261-88) was used at the specified temperature and conditions according to the manufacturer's instructions.

siRNA assays

For HEK293T cells, scrambled siRNAs (scRNA, control) or siRNAs for ZDHHCs were transfected into cells using Lipofectamine 3000 (Invitrogen, L3000–015) according to manufacturer's instructions. For THP-1 cells, siRNAs were electroporated using the Neon Transfection System (Invitrogen, NEON1), and the cells were grown for 48 h before

conducting any further experiments. The parameters for electroporation were as follows: voltage (V) of 1400, pulse width (ms) of 20, pulse number of 2, and the buffer provided with the Neon Transfection System was used (buffer R and buffer E or buffer E2).

Detailed information on siRNAs is as follows. *ZDHHC5* siRNA: ON-TARGETplus Human ZDHHC5 (25921) siRNA, SMARTpool (Horizon Discovery, L-026577–01-0005); *ZDHHC9* siRNA: ON-TARGETplus Human ZDHHC9 (51114) siRNA, SMARTpool (Horizon Discovery, L-021011–01-0005); control siRNA: ON-TARGETplus Non-targeting Pool (Horizon Discovery, D-001810–10-05); *ZDHHC12* siRNA (Thermo Fisher Scientific, 131467); *ZDHHC17* siRNA (Thermo Fisher Scientific, 140245); *ZDHHC20* siRNA (Thermo Fisher Scientific, 141601); *ZDHHC21* siRNA (Thermo Fisher Scientific, 130006).

Non-reducing SDS–PAGE

Cells were lysed in buffer A without a reducing agent and prepared with reducing agent-free SDS loading buffer. The samples were electrophoresed through a 4–16% native PAGE Bis-Tris gel (Invitrogen) in native PAGE running buffer (Invitrogen) at 4 °C and 150 V. Proteins were transferred to PVDF membranes at 0.2 A for 1 h followed by immunoblotting.

Immunoblot analysis

Cells (including cell debris in the supernatant) were collected and lysed using lysis buffer (50 mM Tris-HCl pH 7.4, 150 mM NaCl, 1% NP40 supplemented with Halt protease inhibitor cocktail (Sigma-Aldrich, S8830–20Tab). The samples were incubated for 2 h with gentle rotation at 4 °C and then centrifuged at 20,000*g* for 20 min. The supernatant was collected and the Pierce BCA Protein Assay Kit (Thermo Fisher Scientific, 23225) was used to determine the protein concentration to equalize the amounts of proteins in all of the samples. The samples were processed for SDS–PAGE on 4–15% Mini-PROTEAN TGX Precast Protein Gels (Bio-Rad) and transferred to a 0.2 μm nitrocellulose membrane using the iBlot system (Invitrogen) followed by blocking with 5% milk in Tris-buffered saline with Tween-20 (TBST) for 30 min. After blocking, the membrane was washed three times using TBST, 5 min each. For anti-Flag immunoblotting, the membrane was incubated with 1:1,000 mouse monoclonal anti-Flag M2-peroxidase (HRP) antibodeis (Sigma-Aldrich, A8592) for 3 h at room temperature or overnight at 4 °C. For all other immunoblots, they were probed with the following antibodies: 1:1,000 rabbit anti-GSDMD monoclonal antibody (Cell Signaling Technology, CST-39754), 1:1,000 rabbit anti-GSDMD polyclonal antibody (Novus Biologicals, NBP-33422), 1:500–1,000 rabbit anti-ZDHHC5 polyclonal antibody (Proteintech, 21324–1-AP), 1:500–1,000 rabbit anti-ZDHHC9 polyclonal Antibody (ABclonal, A7977), 1:1,000 rabbit anti-calnexin antibody (Cell Signaling Technology, 2433S), 1:1,000 rabbit anti-COX IV (3E11) monoclonal antibody (Cell Signaling Technology, 4850T), 1:1,000 goat anti-IL-1β polyclonal antibody (R&D Systems, AF-201-NA), 1:1,000 rabbit anti-APT1 polyclonal antibody (Proteintech, 16055–1-AP), 1:1,000 rabbit anti-APT2 polyclonal antibody (Novus Biologicals, NBP1–56653), 1:5,000 mouse anti-GAPDH monoclonal antibody (Proteintech, 60004–1-IG), and 1:1,000 mouse anti-β-actin (8H10D10) monoclonal antibody (Cell Signaling Technology, 3700). The membrane was incubated with a primary antibody at 4 °C overnight. The next day, the membrane was washed three times with TBST, 5 min each, and then incubated

with a secondary antibody, 1:1,000 HRP-goat anti-rabbit IgG (Invitrogen, 31460) or 1:1,000 HRP-goat anti-mouse IgG (Invitrogen, 31432), for 3 h at room temperature. The membrane was rewashed three times with TBST, for 5 min each, and visualized using the SuperSignal West Atto Ultimate Sensitivity Substrate kit (Sigma-Aldrich, A38556). Western blot images were captured using the Bio-Rad Chemidoc MP imaging system and the band intensities were quantified using ImageJ.

Gels used for immunoblotting were as follows: 15-well 4–15% Mini-PROTEAN TGX Precast Protein Gels (Bio-Rad, 4561086); 12-well 4–15% Mini-PROTEAN TGX Precast Protein Gels (Bio-Rad, 4561085); 15-well 4–20% Mini-PROTEAN TGX Precast Protein Gels (Bio-Rad, 4561096); 12-well 4–20% Mini-PROTEAN TGX Precast Protein Gels (Bio-Rad, 4561095).

Immunofluorescence assays

HEK293T cells were plated in 24-well plates with poly-l-lysine coated glass coverslips (12 mm) at 5×10^4 cells per well. After 24 h, these cells were pretreated or not with 2-BP (Sigma-Aldrich, 21604–1G) at 50 μM for 30 min, followed by transfection of appropriate constructs using Lipofectamine 3000 (Invitrogen, L3000008). At 16 h after transfection, cells were treated or not with AMA (Sigma-Aldrich, A8674) at 10 μg ml^{-1}, Rot (Sigma-Aldrich, R8875–1G) at 10 μM, *N*-acetyl cysteine (NAC, Sigma-Aldrich, A9165–25G) at 15 mM, Tiron (Bio Basic TB0951) at 5 mM or MitoT (Sigma-Aldrich, SML0737) at 500 μM for 4 h and fixed by the addition of 500 μl 4% paraformaldehyde in PBS at 37 °C for 15 min. After washing twice with PBS, cells were blocked with 2% bovine serum albumin (BSA) in PBS for 30 min at room temperature. Cells were then permeabilized by adding 500 μl of 0.1% Triton X-100 in 1× PBS and incubated at room temperature for 20 min. After washing twice with PBS, cells were incubated with the mouse monoclonal anti-Flag M2 antibody, diluted 1:500 in PBS buffer containing 2% BSA, at 4 °C in the dark overnight, followed by incubation with Alexa Fluor 555 goat anti-mouse IgG (Invitrogen, A-21422) for 3 h at room temperature. The coverslips were then mounted using ProLong Gold Antifade Mountant with DAPI (Thermo Fisher Scientific, P36941) onto slides and left to dry for 1.5 h in the dark.

For THP-1 *GSDMD*-KO cells or *Gsdmd*-KO iBMDMs, cells were pretreated or not with 2-BP (50 μM) for 30 min, followed by electroporation of appropriate constructs using the Neon Transfection System (Invitrogen). After electroporation, these cells were plated in 24-well plates with poly-l-lysine-coated glass coverslips (12 mm) at 5×10^4 cells per well. At 16 h after electroporation, cells were treated or not with AMA (10 μg ml^{-1}), Rot (10 μM), NAC (15 mM), Tiron (Bio Basic TB0951) at 5 mM or MitoT(Sigma-Aldrich, SML0737) at 500 μM) for 4 h and fixed, blocked and incubated with the appropriate antibodies as described above for HEK293T cells.

All of the images were taken using the Leica TCS SP8 confocal laser-scanning microscope at the Boston Children's Hospital Microscopy Facility. Images were taken with a ×63 objective with a 5.0 or 6.0 zoom factor. The images were identically acquired and processed using Adobe Illustrator or ImageJ software. The quantification was performed on the Leica TCS SP8 confocal laser-scanning microscope (Boston Children's Hospital Microscopy

Facility) for all imaging data by counting about 60 cells in each of the three independent repeats.

Live-cell imaging

GSDMD–GFP- or GSDMD–mCherry-reconstituted *GSDMD*-KO THP-1 cells or iBMDMs were plated in CELLview Cell Culture Dish (Four Compartments, USA Scientific, 5662–7870) and treated with 200 ng ml^{-1} PMA for 48 h. Cells were pretreated or not with 2-BP (50 μM) for 30 min, and treated with AMA (10 μg ml^{-1}), Rot (10 μM), NAC (15 mM), Tiron (5 mM) or MitoT (500 μM) for 4 h, LPS (1 μg ml^{-1}) for 3 h and nigericin (20 μM) for 1 h. After treatment with 1 μg ml^{-1} PI or 0.5 μM Sytox green for 30 min, the cells were then imaged immediately using the Leica TCS SP8 confocal microscope with a 5% CO_2 incubator at 37 °C.

All of the images were taken using the Leica TCS SP8 confocal laser-scanning microscope at the Boston Children's Hospital Microscopy Facility. The large-field images were taken using a ×63 objective with a 2.0 zoom factor and the small-field images was taken by a ×63 objective with a 5.0 or 6.0 zoom factor. The images were identically acquired and processed using Adobe Illustrator or ImageJ. The quantification was performed on the Leica TCS SP8 confocal laser-scanning microscope (Boston Children's Hospital Microscopy Facility) for all imaging data by counting about 60 cells in each of the three independent repeats.

Live-cell ROS measurements

For ROS imaging, cells were manipulated and treated identically under different conditions. 5 μM CellROX Green (Invitrogen, C10444) and 1 μM MitoSOX Red (Invitrogen, M36008) were added to the cells for 30 min at 37 °C. Images were taken on the Inverted Nikon Ti2 fluorescence microscope with a ×40 objective (NA = 1.2) with a stage-top incubator to maintain 37 °C and 5% CO_2. The fluorescence intensities of CellROX Green and MitoSOX Red were determined using ImageJ.

Metabolic labelling in cellulo

Expression of GSDMD–mCherry was performed by transfecting HEK293T cells with 2 μg DNA and Lipofectamine 2000. After 16 h, the medium was replaced with 1 ml DMEM conditioned with 1% charcoal-stripped fatty acid-free BSA. The same medium contained 50 μM 2-BP solubilized in DMSO for 2-BP experiments. Then, 2 h later, the cells were fed with 100 μM saponified fatty acid alkyne 17-octadecynoic Acid (17-ODYA), 100 μM alkyne 15-hexadecynoic acid (15-HDYA) or 25 μM 13-tetradecynoic acid (13-TDYA) dissolved in DMEM conditioned with 20% charcoal-stripped fatty acid-free BSA. After 6 h cells were collected into microfuge tubes with two washes of 1× PBS.

Cells were resuspended in radioimmunoprecipitation assay (RIPA) buffer supplemented with 100× Halt protease inhibitor cocktail and benzonase nuclease, extracted for 90 min with rotation and centrifuged at the maximum speed of a microfuge for 10 min at 4 °C to clarify lysates. The clarified lysate was then subjected to copper-based click chemistry analysis with tetramethyl-rhodamine azide (TAMRA) as reporter group or with biotin-azide for pull-down. Clarified lysate was mixed with 100 μM TAMRA (dissolved in DMSO) and 100 μM Tris

[(1-benzyl-1H-1,2,3-triazol-4-yl) methyl] amine (TBTA), followed by the addition of 1 mM $CuSO_4$ and 1 mM TCEP, dissolved in water. This mixture was allowed to react for 1 h at 37 °C, mixing occasionally. The reaction was quenched by adding 6× SDS–PAGE loading buffer and the sample was separated on precast 4–20% Mini-PROTEAN TGX Precast Protein gels. *S*-acylated proteins, mainly GSDMD due to overexpression, were visualized by detecting fluorescence from the TAMRA channel using a ChemiDoc MP System.

dsDNA and LPS electroporation

A total of 1×10^6 PMA-treated THP-1 cells was electroporated with poly(dA:dT) (1 μg, dsDNA) or LPS (1 μg) using the Neon Transfection System (Invitrogen). After electroporation, cells were plated in an appropriate tissue culture plate, and treated or not with the indicated chemicals 6 h after electroporation. After treatment, cells were ready for appropriate assays. Parameters for electroporation were as follows: voltage (V) of 1400, pulse width (ms) of 20, pulse number of 2, and buffer provided with the Neon Transfection System (buffer R and buffer E or buffer E2).

Active and inactive flatox protein purification and treatment

Active and inactive flatox protein constructs were ordered from Addgene (active flatox, 84871; inactive flatox, 84872). Recombinant active and inactive flatox proteins were purified from *E. coli* as previously described[61]. Endotoxin was removed from these proteins using the Pierce High Capacity Endotoxin Removal Spin Columns (Thermo Fisher Scientific, 88274) according to the manufacturer's protocol. Then, 2 μg ml^{-1} endotoxin-removed active and inactive flatox proteins were mixed with 2 μg ml^{-1} anthrax protective antigen (List Biological Laboratories, 171E) and then were added to iBMDMs. After 6 h, cells were treated or not with indicated chemicals. After treatment, cells were ready for appropriate assays.

HeaTil click chemistry screen for ZDHHCs

A total of 0.25 μg of wild-type human GSDMD–mCherry DNA was aliquoted to multiple 1.5 ml microfuge tubes. Human ZDHHC constructs from the HeaTil screen (1–2 μg)[41] were individually added to each tube and mixed gently. Lipofectamine 2000 was added three times excess to the amount of total DNA and incubated for 20–30 min. This DNA–Lipofectamine mixture was then added to each well of a six-well plate. GSDMD DNA, devoid of ZDHHC, was also transfected as a control to check for background *S*-acylation. Cells were fed with 17-ODYA, collected and clicked as described above. Expression of YFP-tagged ZDHHC and GSDMD proteins were detected by YFP fluorescence and western blot using anti-GSDMD antibody, respectively. Loading controls were determined by western blotting developed using anti-GAPDH antibody.

Mitochondria isolation

Mitochondria were isolated using the Mitochondria Isolation Kit for Cultured Cells (Thermo Fisher Scientific, 89874) according to the manufacturer's instruction. Cells were pelleted by centrifuging at around 850*g* for 2 min. Then, 800 μl reagent A was added, vortexed at medium speed for 5 s and incubated on ice for exactly 2 min. Then, 10 μl mitochondria

isolation reagent B was added. The sample was vortexed at the maximum speed for 5 s and incubated on ice for 5 min with vortexing at maximum speed once every minute. Then, 800 µl mitochondria isolation reagent C was added, and the tube was inverted several times to mix (do not vortex) and centrifuged at 700*g* for 10 min at 4 °C. The supernatant was transferred to a new 2.0 ml tube and centrifuged at 3,000*g* for 15 min at 4 °C. The pellet containing the isolated mitochondria was washed by adding 500 µl mitochondria isolation reagent C and centrifuged at 12,000*g* for 5 min. The pellet was kept on ice before performing ABE.

Negative-stain EM analysis

Palmitoylated full-length GSDMD protein (50 µM) was mixed with liposomes (5 mM lipids) and incubated on ice for 3 h. The samples were diluted in buffer A, applied to glow-discharged Formvar-coated copper grids (Electron Microscopy Sciences), air dried for 60 s, washed with 5 µl buffer A twice, stained with 1% uranyl formate for 60 s and blotted dry. Imaging was performed on the Joel JEM1400 Transmission Electron Microscope (120 keV) at the BCH/PCMM Microscopy Core at Boston Children's Hospital.

Reconstitution and purification of full-length GSDMD pores

1-Palmitoyl-2-oleoyl-*sn*-glycero-3-phosphocholine (PC) was mixed with 1′,3′-bis[1,2-dioleoyl-*sn*-glycerol-3-phospho]-glycerol (CL) (Avanti Polar Lipids) at a molar ratio of 4:1. The solvent chloroform was evaporated under nitrogen gas and resuspended in buffer (40 mM HEPES at pH 7.4, 150 mM NaCl) to a lipid concentration of approximately 5 mM by vigorous vortexing. The formed liposomes were extruded through a 200 nm filter (Whatman Nuclepore) for 35 passes to generate unilamellar vesicles. Purified palmitoylated GSDMD was added at a final concentration of around 50 µM and incubated at room temperature for overnight. The samples were then solubilized by buffer (40 mM HEPES at pH 7.4, 150 mM NaCl) supplemented with 2% C12E8 (Anatrace) to extract GSDMD assemblies. Detergent solubilized GSDMD samples were immediately applied to gel fractionation using the Superose 6 (10/300) Increase size-exclusion column (Cytiva) equilibrated with buffer (40 mM HEPES pH 7.5, 150 mM NaCl and 0.006% C12E8).

Cryo-EM data collection

For cryo-EM grid preparation, purified palmitoylated full-length GSDMD protein samples (3 µl, 0.7 mg ml^{-1}) were applied to glow-discharged 300-mesh Quantifoil gold grids coated with graphene in a Vitrobot (FEI) set at blotting force 0, blotting time 5 s, 100% humidity and 4 °C. The blotted grids were immediately plunged into liquid ethane and transferred to liquid nitrogen for storage. Before data collection, all of the grids were prescreened using a Talos Arctica microscope (Thermo Fisher Scientific) operating at 200 keV equipped with Gatan K3 direct electron detector at Harvard Cryo-EM Center for Structural Biology (HC^2EM) to achieve good ice and particle quality. The datasets were collected at HC^2EM using a Titan Krios microscope (Thermo Fisher Scientific) operating at an acceleration voltage of 300 keV equipped with BioQuantum K3 imaging filter (Gatan; slit width, 20 eV). The data collection was operated in super-resolution mode with 105,000 magnification (0.415 Å per pixel) and a defocus range between −1.0 and −2.0 µm. For each image stack

with 60 frames, the total dose was 60.0 electrons per Å^2. SerialEM (v.3.8)[62] was used for fully automated data collection.

For full-length, palmitoylated GSDMD pore grid preparation, 3 μl (0.5 mg ml^{-1}) purified pore samples were applied to plasma glow-discharged 300-mesh gold lacey carbon grids coated with ultrathin carbon film (Ted Pella), using the Vitrobot (FEI) set at 100% humidity and 4 °C. The grid was then blotted with filter paper for 5 s at blotting force 8 after a waiting time of 5 s. Blotted grids were immediately plunged into liquid ethane and transferred to liquid nitrogen for storage. Before data collection, all of the grids were prescreened using the Talos Arctica microscope (Thermo Fisher Scientific) operating at 200 keV equipped with the Gatan K3 direct electron detector at the Harvard Cryo-EM Center for Structural Biology (HC^{2}EM) to achieve a good ice and particle quality. The datasets were collected at HC^{2}EM using the Titan Krios microscope (Thermo Fisher Scientific) operating at an acceleration voltage of 300 keV equipped with a BioQuantum GIF/K3 direct electron detector. The data collection was operated in super-resolution mode with 130,000 magnification (0.47 Å per pixel) and a defocus range between −0.8 and −2.2 μm. For each image stack with 48 frames, the total dose was 55.26 electrons per Å^2. SerialEM (v.3.8)[62] was used for fully automated data collection.

Cryo-EM data processing

The computer support and software for data processing support were provided by the SBGrid consortium[63]. Datasets were processed in cryoSPARC[64].

For monomeric palmitoylated GSDMD structure, raw videos were corrected for motion by patch motion correction in cryoSPARC, followed by particle picking in Blob Picker. A total of 930,908 particles was picked. 2D classification was performed followed by selection of good particles from 2D classes. In total, 803,205 particles were selected and processed for 3D classification into 3 classes. Homogeneous refinement with C_1 symmetry was performed to obtain the final map at 5.3 Å resolution determined by Fourier shell correlation. Model fitting was performed in ChimeraX[65] using the unpalmitoylated GSDMD structure (PDB: 6N9O)[12] as the starting point.

For full-length GSDMD pore, raw videos were corrected by gain reference and beam-induced motion with or without dose weighting using the Relion v.4.01 implementation of the MotionCor2 algorithm[66,67]. The motion-corrected micrographs were imported into cryoSPARC, followed by particle picking in Blob Picker. A total of 3,590,814 particles was extracted. Multiple rounds 2D classification was performed to select good particles from 2D classes. In total, 108,946 particles were selected and processed for ab initio reconstruction to get the initial model. Heterogeneous refinement with C_1 symmetry was performed to further remove bad particles. A total of 55,274 particles was used to do non-uniform refinement with C_{33} symmetry and obtain the final map at 5.5 Å resolution determined by Fourier shell correlation. Model fitting was performed in ChimeraX[65] using the GSDMD-NT pore structure (PDB: 6VFE) and pre-pore map[8] as the starting point. Structural figures were generated in Pymol[68] and ChimeraX[65]. The figure schematic was created using BioRender.

Liposome leakage assay

Expression and purification of mammalian and bacterial GSDMD and their mutants have been described above. To generate depalmitoylated GSDMD for liposome leakage assays, recombinant GSDMD was incubated with 0.7 M HA for 1 h at room temperature, and buffer-exchanged five times to remove HA using a 10 kDa MWCO concentrator (EMD Millipore) and 20 mM HEPES at pH 7.4, 150 mM NaCl. To produce oxidized GSDMD, purified recombinant bacterial GSDMD was oxidized with H_2O_2 as previously described[69]. In brief, GSDMD was incubated with H_2O_2 for 30 min in PBS buffer at room temperature. Subsequently, the sample was dried using a lyophilizer (Labconco) and used subsequently.

Liposomes were prepared as previously described[8,47]. In brief, phosphatidylcholine (1-palmitoyl-2-oleoyl-*sn*-glycero-3-phosphocholine, 25 mg ml^{-1} in chloroform; 80 µl), PE (1-palmitoyl-2-oleoyl-*sn*-glycero-3-phosphoethanolamine, 25 mg ml^{-1} in chloroform; 128 µl) and cardiolipin (CL, 1′,3′-bis(1,2-dioleoyl-*sn*-glycero-3-phospho)-*sn*-glycerol (sodium salt), 25 mg ml^{-1} in chloroform; 108 µl) were mixed and the solvent was evaporated under a stream of N_2 gas. The lipid mixture was suspended in 1 ml buffer A (20 mM HEPES at pH 7.4, 150 mM NaCl, 50 mM sodium citrate and 15 mM $TbCl_3$) for 3 min. The suspension was pushed through 100 nm Whatman Nuclepore Track-Etched Membrane 30 times to obtain homogeneous liposomes. The filtered suspension was purified by a size-exclusion column (Superose 6, 10/300 GL) in buffer B (20 mM HEPES, 150 mM NaCl) to remove $TbCl_3$ outside liposomes. Void fractions were pooled to produce a stock of PC/PE/CL liposomes (1.6 mM). Expression and purification of catalytically active CASP1 were performed using the previously reported refolding method[70]. In brief, two non-tagged p20 and p10 subunits were expressed in *E. coli* BL21 (DE3) bacteria in inclusion bodies individually. The p20–p10 complex was assembled by denaturation and refolding, and was further purified by HiTrap SP cation-exchange chromatography (GE Healthcare Life Sciences).

The liposomes were diluted 10 times (the baseline of empty liposome is about 35 RFU) with buffer C (20 mM HEPES, 150 mM NaCl and 15 µM DPA) for use in a liposome leakage assay in which the leakage of Tb^{3+} from inside the liposomes was detected by an increase in fluorescence when Tb^{3+} was bound to dipicolinic acid (DPA) in buffer C. Human GSDMD (0.5 µM, WT or C191A mutant), bacterially produced or Expi293 expressed, was precleaved by 3C for 30 min or CASP1 for 1 h, and added to 384-well plates (Corning, 3820) containing PC/PE/CL liposomes (50 µM liposome lipids). For liposome leakage assays of intact GSDMD, the precleavage step was skipped. The fluorescence intensity of each well was measured at 545 nm using excitation at 276 nm immediately after mixing and followed for 40 min or 2 h using a SYNERGY microplate reader (Biotek). The emission fluorescence at 545 nm before adding the protein was treated as F_0. After 40 min or 2 h, 1% Triton X-100 was added to achieve complete release of Tb^{3+}. The mean values of the top three fluorescence reads were defined as F_{100}. The percentage of Tb^{3+} release at each timepoint is defined as follows: Tb^{3+} release (%) = $(F - F_0) \times 100/(F_{100} - F_0)$.

GSDMD and ZDHHS expression

ZDHHS represents the catalytically inactive mutant of ZDHHC in which the catalytic Cys is mutated to Ser. Expi293 cells were seeded at approximately 1×10^6 cells per ml maintained in 50 ml Expi293 expression medium and grown in an orbital shaker incubator at 37 °C, 105 rpm and 5% CO_2 until cells reached a density of 2×10^6 cells per ml. Cells were transiently transfected with 50 μg of DNA: *GSDMD* (25 μg) and *ZDHHS5/9/12/17/20* (25 μg). *GSDMD* DNA devoid of *ZDHHS*, and *ZDHHS* DNA devoid of *GSDMD* were also transfected as controls to check for background resin binding. For transfection, DNA, purified in water, was mixed with PEI, at a ratio of 1:3 (DNA:PEI) in Expi293 expression medium. After 30 min, the DNA–PEI mixture was added to the cells and grown in an orbital shaker incubator. Then, 12 h after transfection, cells were fed with filtered 45% d-(+)-glucose and 10 mM sodium butyrate solution. Cells were left to incubate for an additional 48 h. Cells were collected with one wash of 1× PBS at 2,500 rpm for 30 min at 4 °C.

GSDMD and ZDHHS co-immunoprecipitation

GSDMD and ZDHHS cell pellets were thawed on ice and resuspended in ice-cold cell lysis buffer (1× PBS pH 7.4, 1 mM TCEP, 1 mM EDTA, 10% glycerol and 0.5% Triton X-100) supplemented with 100× Halt protease inhibitor cocktail and benzonase nuclease. Cells were left to rotate for 90 min at 4 °C and centrifuged at maximum speed for 10 min. The whole-cell lysate was incubated with washed anti-Flag M2 Affinity Gel (Sigma-Aldrich, A2220–4X25ML) at 4 °C for 2 h on an end-over-end rotator. The samples were centrifuged in a microcentrifuge at 500*g* for 2 min at 4 °C and the flow through was collected with a pipettor. Beads were washed three times with ice-cold wash buffer 1 (1× PBS pH 7.4, 1 mM TCEP, 1 mM EDTA, 5% glycerol and 0.5% Triton X-100). Beads were washed a final time with ice-cold wash buffer 2 (1× PBS pH 7.4, 1 mM EDTA, 5% glycerol and 0.5% Triton X-100). The samples were eluted by incubating at room temperature on a shaking rack for 5 min with elution buffer (1× PBS pH 7.4, 1 mM EDTA, 5% glycerol, 0.5% Triton X-100 and 150 ng μl^{-1} 3× Flag peptide) and centrifuged at 500*g* in a microcentrifuge for 1 min. The supernatant was carefully collected with a pipettor and transferred to a clean microcentrifuge tube appropriately labelled with the sample and fraction number. Elution was repeated four more times. The fractions were then separated by SDS–PAGE and analysed by western blotting for GSDMD (anti-Flag) and ZDHHC5 or ZDHHC9.

Quantification and statistical analysis

Statistical significance was calculated using GraphPad Prism 9 (unpaired Student's *t*-tests; https://www.graphpad.com/scientific-software/prism/) or OriginPro (2021, v.9.8). The number of independent experiments of duplicates, the statistical significance and the statistical test used to determine the significance are indicated in each figure, figure legend or Methods section where quantification is reported.

Extended Data

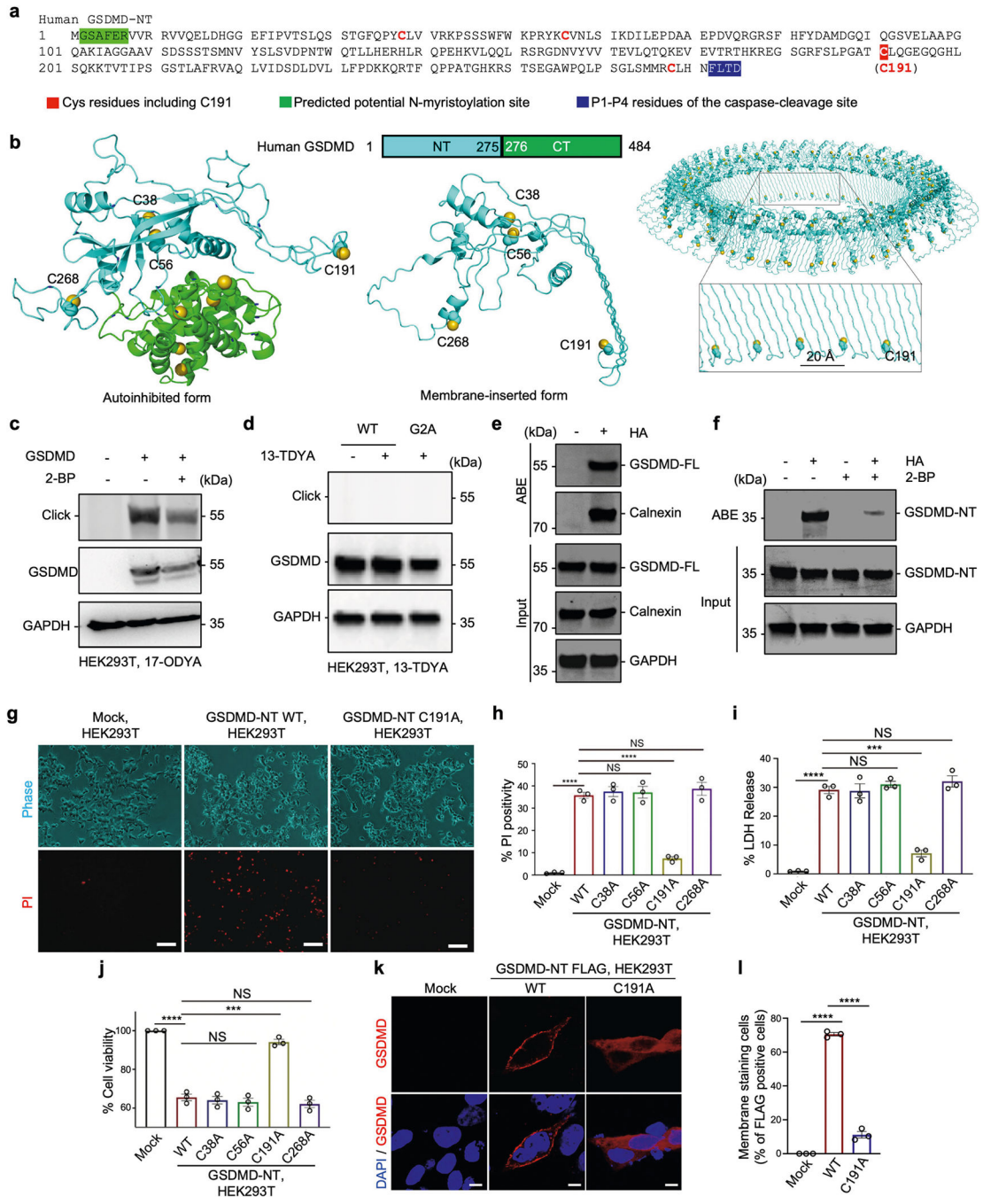

Extended Data Fig. 1 |. GSDMD is palmitoylated at its N-terminus at Cys191.

a, Protein sequence of human GSDMD N-terminal domain (GSDMD-NT). Certain residues are marked by colours. **b**, Domain organization and ribbon diagrams of autoinhibited full-length (FL) GSDMD (modelled after PDB 6N9O, left), membrane-inserted GSDMD-NT monomer (middle), and the GSDMD-NT pore oligomer modelled after PDB 6VFE (right). **c**, GSDMD-FL palmitoylation detected by alkyne stearic acid and rhodamine azide, and

its inhibition by the general palmitoylation inhibitor 2-BP. **d**, Click chemistry for protein N-myristoylation did not detect N-myristoylation of GSDMD using the alkyne-myristate 13-TDYA. **e**, GSDMD-FL palmitoylation when expressed in HEK293T cells detected by ABE, with the known palmitoylated protein Calnexin as a positive control. **f**, GSDMD-NT palmitoylation when expressed in HEK293T cells, detected by ABE, and its inhibition by 2-BP. GAPDH acts as the loading control. **g-l**, PI staining (**g**), PI positivity (**h**), LDH release (**i**), cell viability (**j**), anti-FLAG immunofluorescence imaging for membrane localization (**k**), and its quantification (**l**) of HEK293T cells expressing GSDMD-NT WT or Cys mutants, showing the impairment of C191A in inducing pyroptosis. Scale bars represent 50 μm (**g**) and 5 μm (**l**). Data are presented as the mean ± SEM, n = 3 (**h**-**j**, **l**). (**c**-**f**) Representative of ≥3 independent experiments. Statistics were measured by two-tailed Student's t-tests with NS (non-significant) for $p > 0.05$, *** for $p < 0.001$, and **** for $p < 0.0001$. Immunoblots were incubated with 1:1000 anti-FLAG® M2-peroxidase (HRP) antibody, 1:1000 anti-calnexin antibody, and 1:5000 anti-GAPDH antibody for GAPDH loading controls.

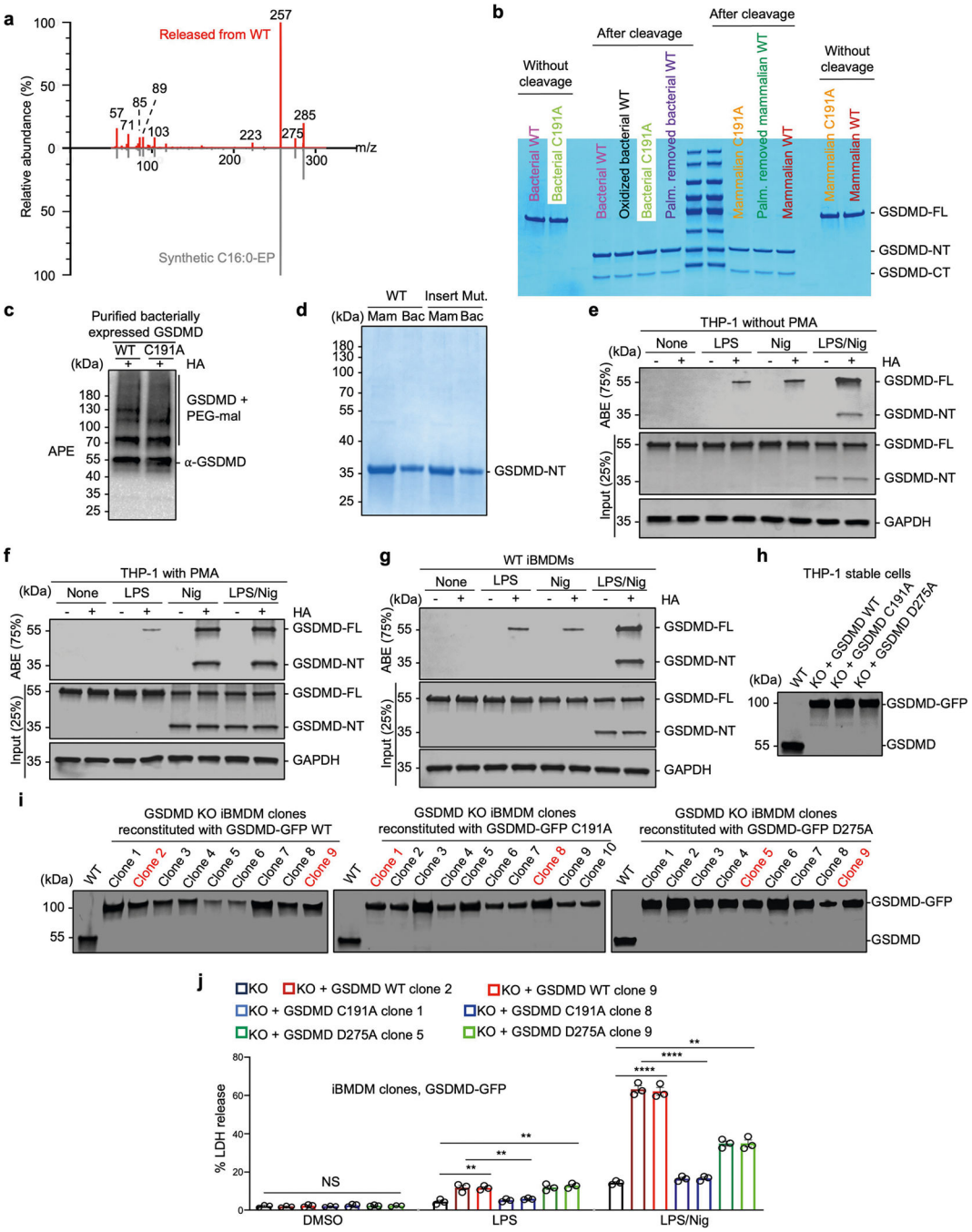

Extended Data Fig. 2 |. GSDMD palmitoylation at Cys191 and its functional effects, and cell death of WT and mutant iBMDMs.

a, UPLC-MS/MS analysis of released ethyl palmitoyl group from Expi293-expressed WT GSDMD (top half, red) and synthetic C16 ethyl palmitate control (bottom half, grey). **b**, Inputs and cleavage of bacterial expressed and mammalian expressed GSDMD proteins used in liposome leakage assays. All proteins were cleaved equally. **c**, APE of bacterially expressed recombinant GSDMD, WT and its C191A mutant, detected by the anti-GSDMD antibody CST-39754. Although each PEG-mal used was 10 kDa in size, the molecular

weight shift it caused was about twice, as noted previously[50]. **d**, Liposome pelleting assay. GSDMD insertion mutant (F184D/L186D) was designed from the GSDMD pore structure[8], which should bind to the membrane but does not fully insert into the membrane to form pores. Even at the high concentration used (35 μM) to enable detection by Coomassie staining, the role of palmitoylation in membrane association was apparent. **e**,**f**, ABE of undifferentiated THP-1 monocytes (**e**) or PMA-differentiated THP-1 macrophages (**f**) treated by LPS, nigericin, or LPS plus nigericin. For differentiated THP-1 cells, nigericin alone and LPS plus nigericin both induced GSDMD cleavage and palmitoylation. **g**, Palmitoylation by ABE of WT iBMDMs upon treatment by LPS, nigericin, or LPS plus nigericin. **h**, Western blot of GSDMD in WT THP-1 and in GSDMD KO THP-1 stably reconstituted with GSDMD-GFP by lentiviruses. Expression levels of GSDMD-GFP in reconstituted THP-1 cells were equal to endogenous GSDMD in WT THP-1 cells. **i**, Western blot of GSDMD in WT iBMDMs and GSDMD KO iBMDM clones stably reconstituted with GSDMD-GFP (WT, C191A, or D275A). Clones of GSDMD-GFP reconstituted iBMDMs with equal expression levels to endogenous GSDMD in WT iBMDMs were selected. The selected clones are labelled in red. **j**, LDH release of GSDMD KO iBMDMs reconstituted with WT, C191A, or D275A GSDMD-GFP upon treatment by LPS and nigericin. All results were obtained from at least 3 independent experiments. Error bars represent SEM. Statistics were measured by two-tailed Student's t-tests with NS (non-significant) for $p > 0.05$, ** for $p < 0.01$, *** for $p < 0.001$, and **** for $p < 0.0001$. Immunoblots were incubated with 1:1000 anti-GSDMD antibody.

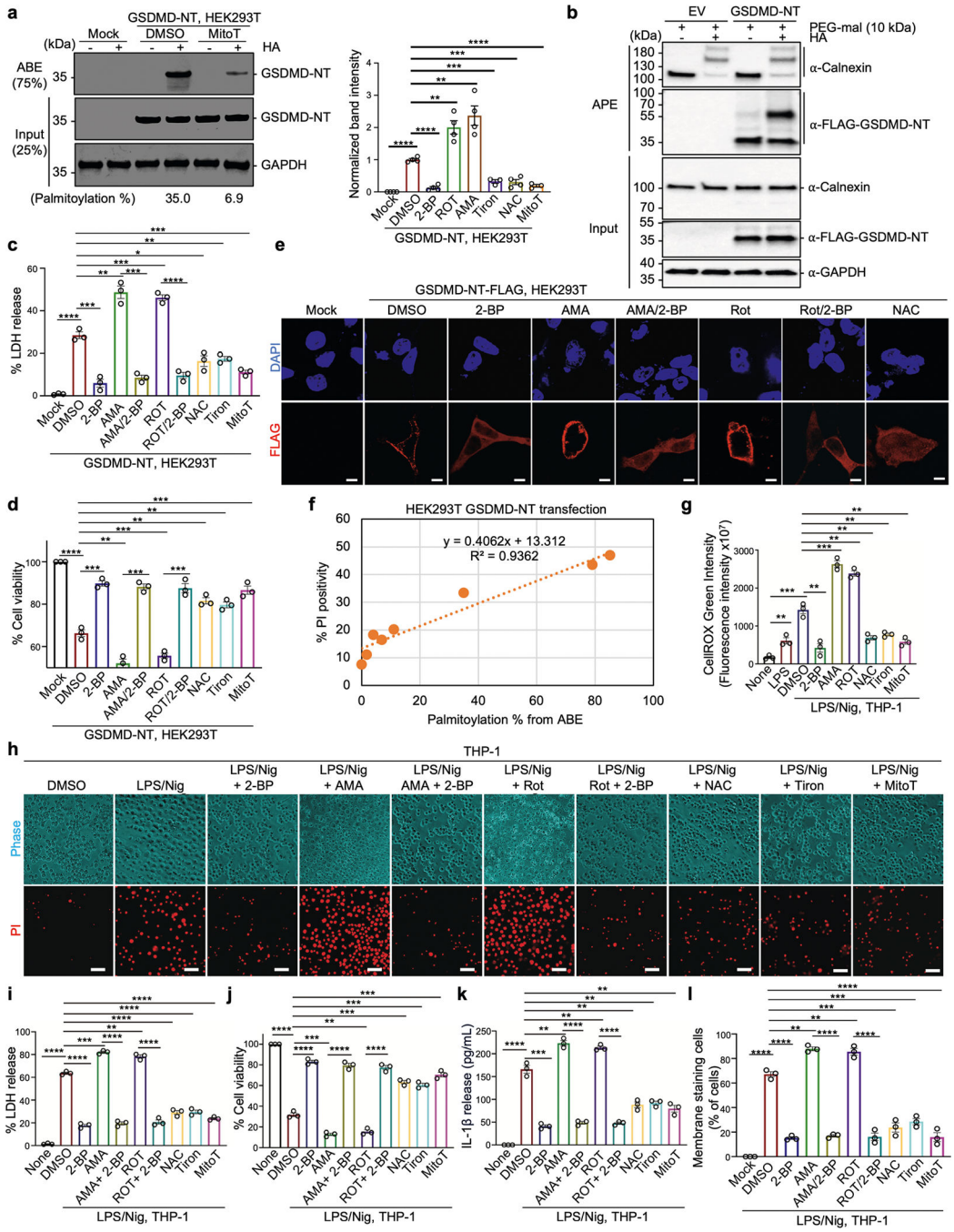

Extended Data Fig. 3 |. Regulation of GSDMD palmitoylation and pyroptosis by ROS modulators.

a, GSDMD-NT palmitoylation detected by ABE and quantified in HEK293T cells expressing GSDMD-NT treated or not ROS activators or quenchers. **b**, GSDMD-NT and calnexin palmitoylation detected by APE in HEK293T cells expressing GSDMD-NT or empty vector. Although the PEG-mal used was 10 kDa in size, the molecular weight shift it caused is roughly twice, as noted previously[50]. **c**, **d**, LDH release (**c**), and cell viability (**d**) of HEK293T cells expressing GSDMD-NT and treated or not with ROS modulators.

e, Anti-FLAG immunofluorescence imaging of HEK293T cells expressing GSDMD-NT and treated with ROS modulators, showing increased cell membrane localization by Rot and AMA and its inhibition by 2-BP, as well as the diffuse cytoplasmic localization upon treatment by NAC. Nuclei are marked by the DNA dye DAPI. Scale bars represent 5 μm. **f**, Plot of PI positivity against % GSDMD palmitoylation, showing an approximately linear relationship. **g**, Measurement of cellular oxidative stress by CellROX in THP-1 cells treated or not with LPS plus nigericin, and with ROS and palmitoylation modulators. **h**-**l**, PI staining (**h**), LDH release (**i**), cell viability (**j**), IL-1β secretion (**k**), and membrane staining (**l**) of THP-1 cells treated or not with LPS + nigericin and with ROS modulators. Scale bar represent 50 μm (**h**). All results were obtained from at least 3 independent experiments. Error bars represent SEM. Statistics were measured by two-tailed Student's t-tests with * for $p < 0.05$, ** for $p < 0.01$, *** for $p < 0.001$, and **** for $p < 0.0001$. Scale bars represent 5 μm (**e**) and 50 μm (**h**). Immunoblots were incubated with 1:1000 anti-FLAG® M2-peroxidase (HRP) antibody, 1:1000 anti-calnexin antibody, and 1:5000 anti-GAPDH antibody for GAPDH loading controls.

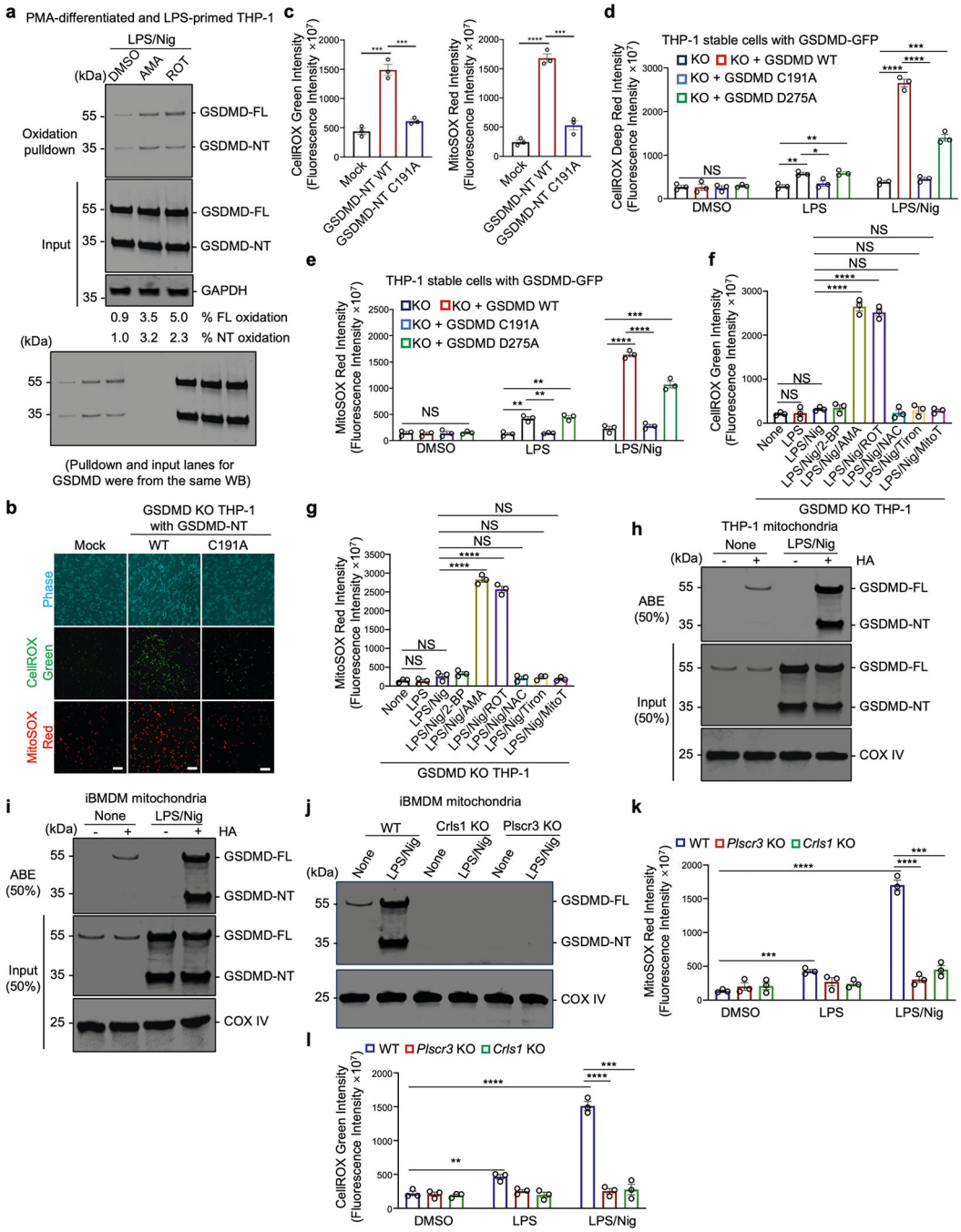

Extended Data Fig. 4 |. GSDMD targets the mitochondria to induce ROS.

a, Pulldown of proteins with oxidized Cys residues in LPS primed and nigericin activated THP-1 cells followed by anti-GSDMD western blot (top). GSDMD is minorly oxidized in primed and activated cells even with additional ROS activators (≤5%). The pulldown and the input lanes were run on the same gel (bottom). **b**,**c**, Imaging (**b**) and quantification (**c**) of cellular oxidative stress by CellROX and MitoSOX in GSDMD KO THP-1 cells electroporated with GSDMD-NT WT or C191A. WT GSDMD-NT expression leads to higher cellular oxidative stress than C191A mutant. Data are presented as the mean ± SEM,

n = 3. Scale bars represent 80 μm (**b**). **d**,**e**, Measurement of cellular and mitochondrial stress by CellROX (**d**), and MitoSOX (**e**) intensity in GSDMD KO THP-1 cells reconstituted with WT, C191A, or D275A (cleavage deficient) GSDMD upon treatment by DMSO, LPS or LPS and nigericin. C191A GSDMD-reconstituted cells did not enhance ROS production upon stimulation by LPS and nigericin as compared to WT GSDMD, while D275A GSDMD-reconstituted cells showed significantly enhanced ROS production. Expression levels of GSDMD-GFP in reconstituted THP-1 cells were equal to endogenous GSDMD in WT THP-1 cells. Data are presented as the mean ± SEM, n = 3. **f**,**g**, Measurement of cellular oxidative stress by CellROX (**f**), and MitoSOX (**g**) of GSDMD KO THP-1 cells treated with LPS, LPS and nigericin, or with additional ROS activators or quenchers, highlighting the GSDMD dependence of ROS generation during inflammasome activation. Data are presented as the mean ± SEM, n = 3. **h**,**i**, Palmitoylated GSDMD detected by ABE in isolated mitochondria from THP-1 cells (**h**) and iBMDMs (**i**) before and after inflammasome activation. **j**, Western blots of GSDMD in isolated mitochondria from WT iBMDMs, *Crls1* KO iBMDMs, or *Plscr3* KO iBMDMs, showing lack of GSDMD in mitochondria from the KO cells. **k**,**l**, ROS measured by MitoSox (**k**) or CellRox (**l**) showing close to baseline ROS in the KO iBMDMs even upon inflammasome activation, in contrast to WT cells. (**h**-**j**) Representative of ≥3 independent experiments. Data are presented as the mean ± SEM, n = 3. Statistics were measured by two-tailed Student's t-tests with NS (non-significant) for $p > 0.05$, * for $p < 0.05$, ** for $p < 0.01$, *** for $p < 0.001$, and **** for $p < 0.0001$. All immunoblots were incubated with 1:1000 anti-GSDMD antibody, and 1:1000 anti-COX IV antibody for COX IV loading controls.

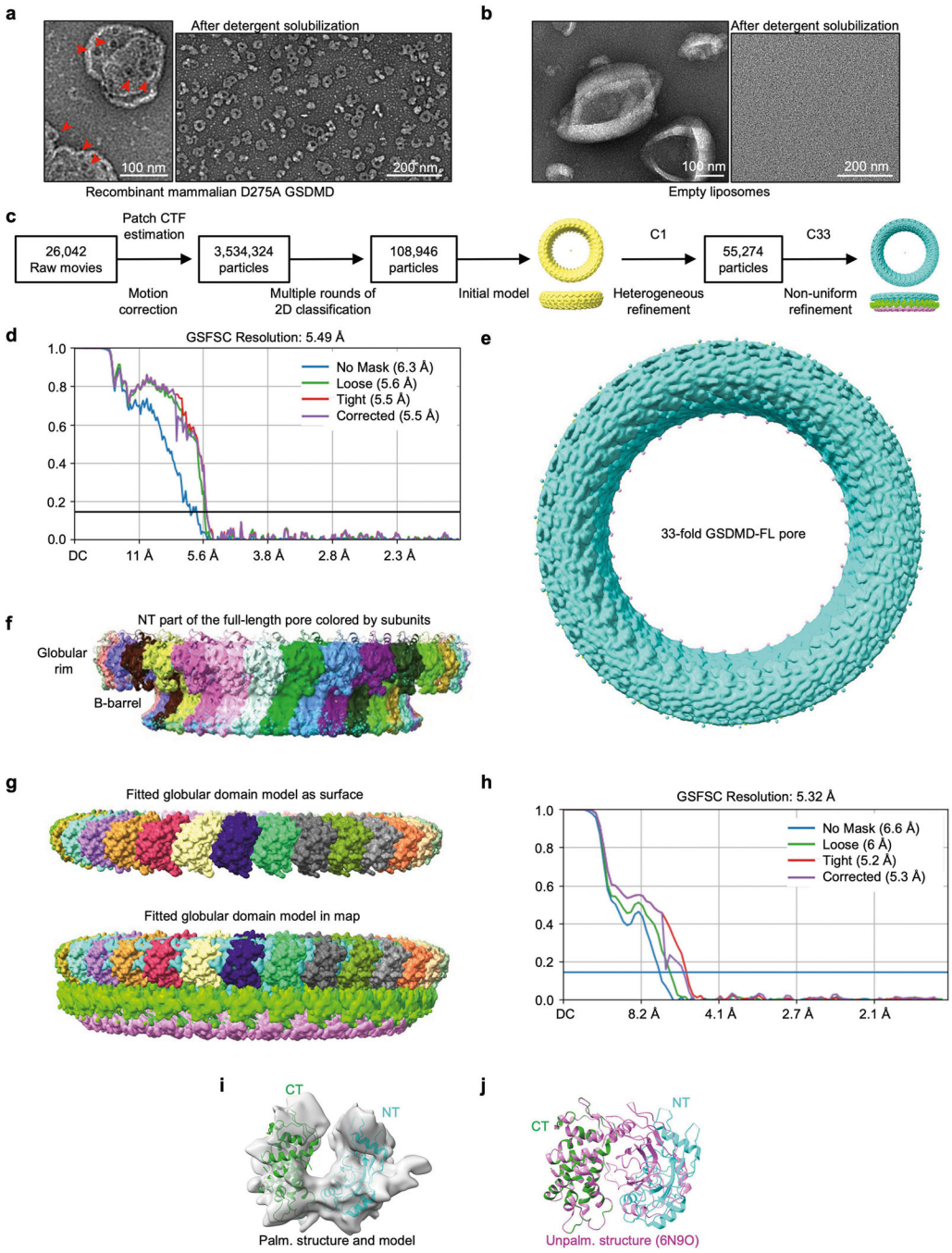

Extended Data Fig. 5 |. Cryo-EM structure of palmitoylated, full-length GSDMD.

a,**b**, Negative staining EM images of GSDMD pores by D275A GSDMD-FL (**a**), or empty liposomes (**b**) on liposomes (left) and after detergent solubilization (right). Red arrowheads indicate a few examples of pores. **c**, Cryo-EM workflow of GSDMD-FL pore structure. **d**, FSC curve of the cryo-EM reconstruction. **e**, Overall view of the cryo-EM density segmented to show GSDMD-NT in cyan. **f**, The globular rim of the GSDMD-NT structure is higher, shown by the ribbon diagram extending above the cryo-EM density of the GSDMD-NT region of the GSDMD-FL pore. **g**, The globular rim domain assembly in the pre-pore

structure of GSDMD-NT (top) and its fitting into the density of full-length GSDMD pore. **h**, FSC curve for the cryo-EM structure of palmitoylated GSDMD. The resolution is likely over-estimated as we cannot visualize individual helices in the map. **i**, **j**, Cryo-EM map of palmitoylated GSDMD (grey) fitted separately with NT (cyan) and CT (green) from unpalmitoylated GSDMD structure (PDB: 6N9O) (**i**), and the comparison of the palmitoylated model with the unpalmitoylated GSDMD structure (**j**). The NT-CT interaction is less compact in the palmitoylated GSDMD structure, suggesting partial overcome of autoinhibition.

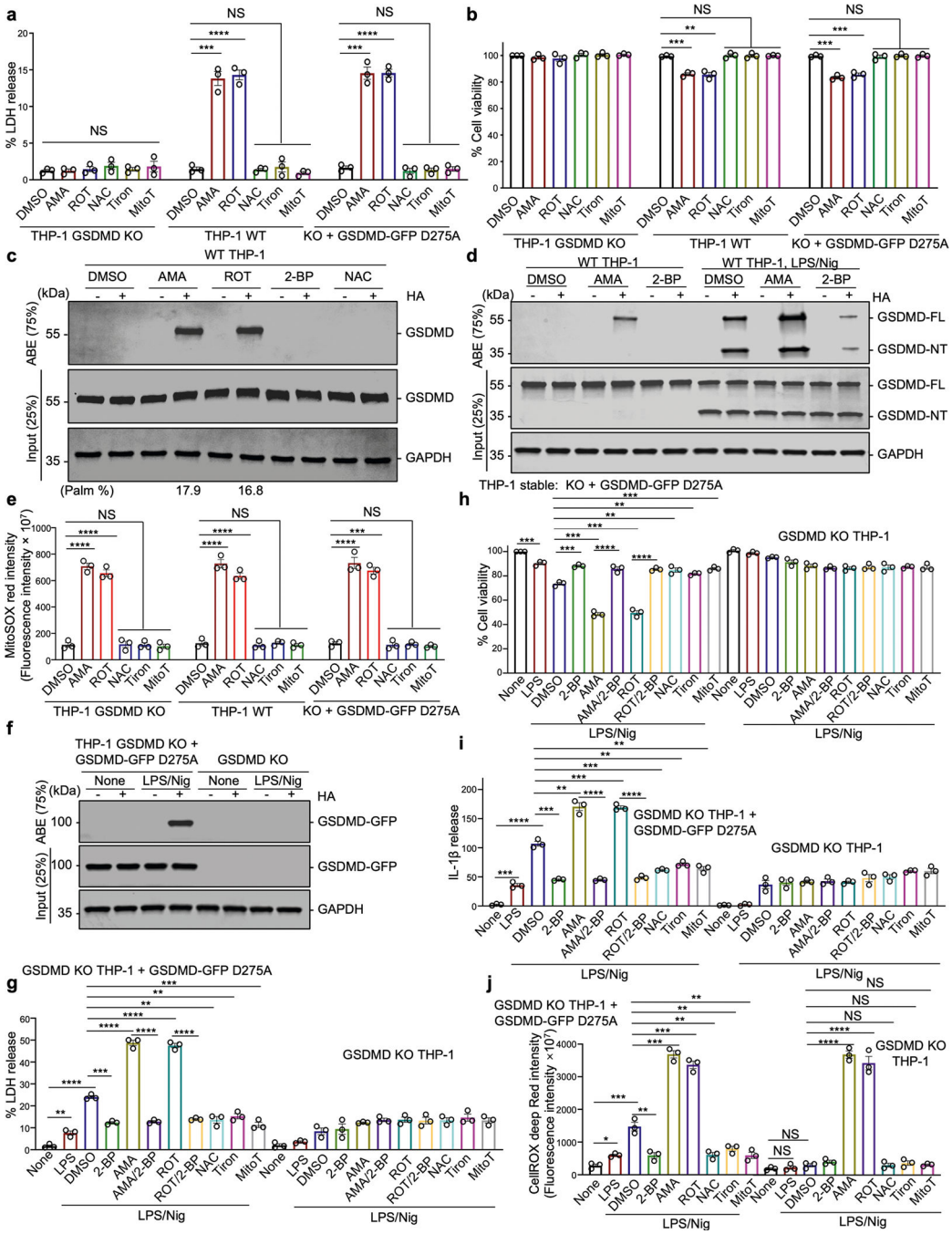

Extended Data Fig. 6 |. GSDMD KO THP-1 cells with uncleavable D275A GSDMD-FL induced ROS, pyroptosis, and membrane localization, and a GSDMD disease mutant enhanced cell death in a palmitoylation-dependent manner.

a,**b**, ROS activators alone induced significant LDH release (**a**) and reduced cell viability (**b**) in GSDMD KO THP-1 stably reconstituted with GSDMD-GFP D275A or WT GSDMD. Expression levels of GSDMD-GFP in reconstituted THP-1 cells were equal to endogenous GSDMD in WT THP-1 cells. **c**,**d**, Palmitoylation in THP-1 cells treated or not with ROS activators or quencher (**c**), or primed and activated and treated or not with ROS activators or quencher (**d**). **e**-**j**, ROS measured by MitoSox (**e**), palmitoylation (**f**), LDH release (**g**),

cell viability (**h**), IL-1β release (**i**), and cellular ROS (**j**) in GSDMD KO THP-1 cells or GSDMD KO THP-1 cells reconstituted with D275A, treated or not with ROS activators or quenchers. Expression levels of GSDMD-GFP in reconstituted THP-1 cells were equal to endogenous GSDMD in WT THP-1 cells. All results were obtained from at least 3 independent experiments. Error bars represent SEM. Statistics used two-tailed Student's t-tests, with NS (non-significant) for $p > 0.05$, ** for $p < 0.01$, *** for $p < 0.001$, and **** for $p < 0.0001$. Immunoblots were incubated 1:5000 anti-GAPDH antibody for GAPDH, and 1:1000 anti-GSDMD antibody.

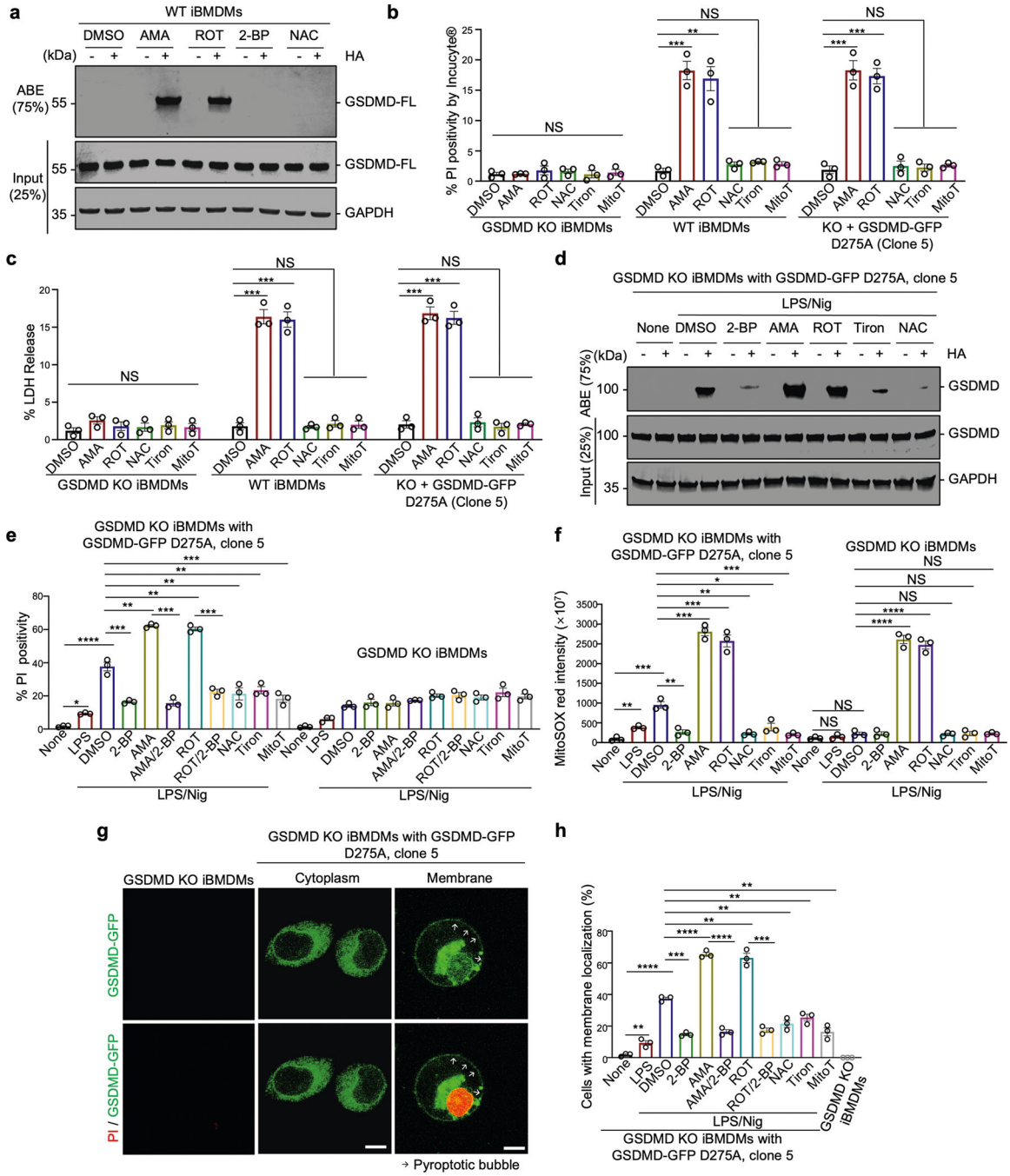

Extended Data Fig. 7 |. GSDMD KO iBMDMs reconstituted with uncleavable D275A GSDMD-FL induce ROS, pyroptosis, and membrane localization upon inflammasome activation and/or ROS activators.

a, Palmitoylation in iBMDMs treated or not with ROS activators or quencher. **b**,**c**, ROS activators alone induced significant PI positivity as measured by Incucyte® (**b**) and increased LDH release (**c**) in GSDMD KO iBMDMs stably reconstituted or not with GSDMD-GFP D275A or WT GSDMD. **d-f**, Palmitoylation (**d**), PI positivity (**e**), and MitoSOX (**f**) in GSDMD KO iBMDMs reconstituted with GSDMD-GFP D275A, clone 5, activated by LPS and nigericin, and treated or not with additional ROS activators, quenchers, or 2-BP. **g**,**h**,

GFP imaging (**g**) and quantification (**h**) for GSDMD membrane localization in clone 5 of GSDMD KO iBMDMs reconstituted with GSDMD-GFP D275A upon inflammasome activation and with or not ROS modulators and 2-BP. Scale bars represent 5 μm (**g**). All results were obtained from at least 3 independent experiments. GSDMD KO iBMDM clones reconstituted with D275A that had equal expression levels to endogenous GSDMD in WT iBMDMs were selected. Error bars represent SEM. Statistics used two-tailed Student's t-tests, with NS (non-significant) for $p > 0.05$, * for $p < 0.05$, ** for $p < 0.01$, *** for $p < 0.001$, and **** for $p < 0.0001$. Immunoblots were incubated with 1:1000 anti-GSDMD antibody and 1:5000 anti-GAPDH antibody for GAPDH loading controls.

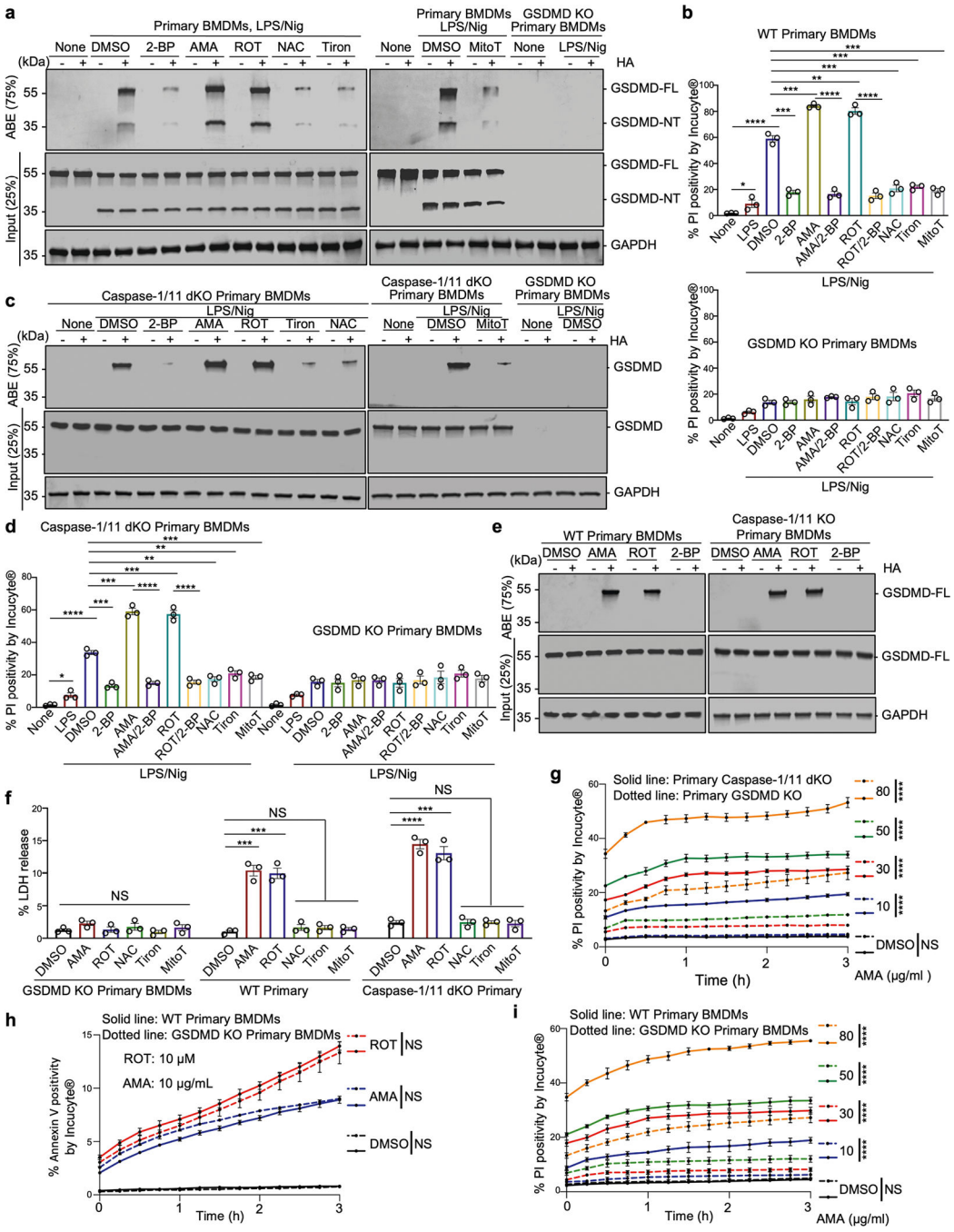

Extended Data Fig. 8 |. Primary BMDMs induce increased palmitoylation and pyroptosis upon inflammasome activation and/or ROS activators.

a-d, Palmitoylation (a,c) and PI positivity (b,d) in primary WT and Gsdmd KO BMDMs (**a**,**b**), or primary caspase-1/11 dKO and Gsdmd KO BMDMs (**c**,**d**) treated or not with 2-BP, ROS activators or quenchers. **e**, GSDMD palmitoylation by ROS activators or 2-BP in primary WT and caspase-1/11 dKO BMDMs. **f**, ROS activators alone increased LDH release in both WT and caspase-1/11 dKO primary BMDMs, but not in Gsdmd KO BMDMs. **g-i**, Time course as measured by Incucyte® of PI (**g**,**i**), or Annexin V positivity (**h**) with ROS

induction without LPS and nigericin treatment in primary WT, Gsdmd KO, and caspase-1/11 dKO BMDMs. All results were obtained from at least 3 independent experiments. Error bars represent SEM. Statistics used two-tailed Student's t-tests, or two-way ANOVA (**g-i**) with NS (non-significant) for $p > 0.05$, * for $p < 0.05$, ** for $p < 0.01$, *** for $p < 0.001$, and **** for $p < 0.0001$. Immunoblots were incubated with 1:1000 anti-GSDMD antibody and 1:5000 anti-GAPDH antibody for GAPDH loading controls.

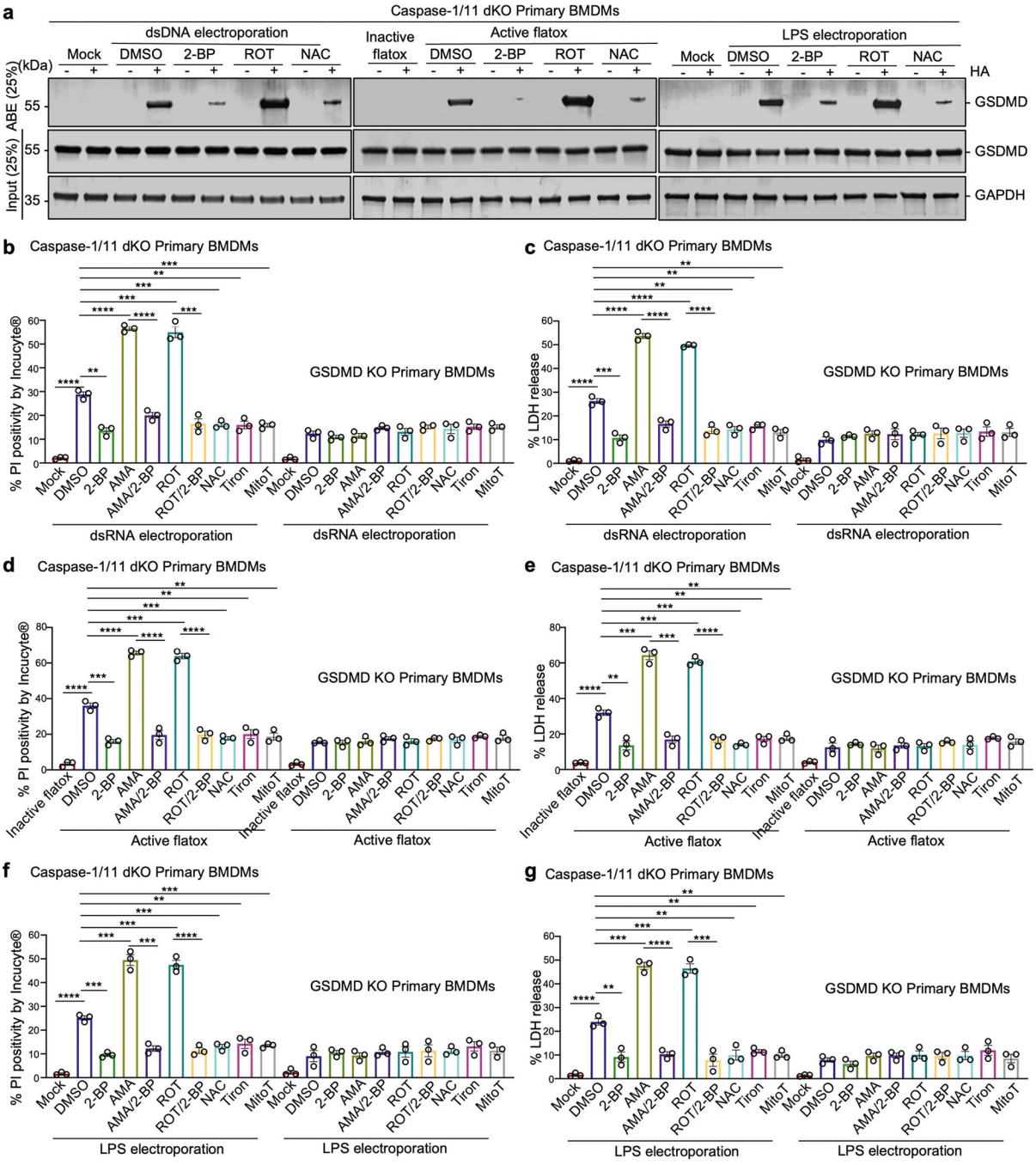

Extended Data Fig. 9 |. GSDMD palmitoylation and cell death in primary BMDMs.

a, GSDMD palmitoylation detected by ABE in primary caspase-1/11 dKO BMDMs upon dsDNA electroporation, flatox treatment or LPS electroporation, and treated or not with ROS activator Rot, 2-BP, or ROS quencher NAC. **b**-**g**, PI positivity (**b**,**d**,**f**) and LDH release (**c**,**e**,**g**) in primary caspase-1/11 dKO BMDMs and primary GSDMD KO BMDMs upon AIM2 inflammasome activation by dsDNA electroporation (**b**,**c**), NAIP5/NLRC4 inflammasome activation by flatox treatment (**d**,**e**), and non-canonical inflammasome activation by LPS electroporation (**f**,**g**). All results were obtained from at least 3 independent experiments. Error bars represent SEM. Statistics were measured by two-tailed Student's t-tests with * for $p < 0.05$, ** for $p < 0.01$, *** for $p < 0.001$, and **** for $p < 0.0001$.

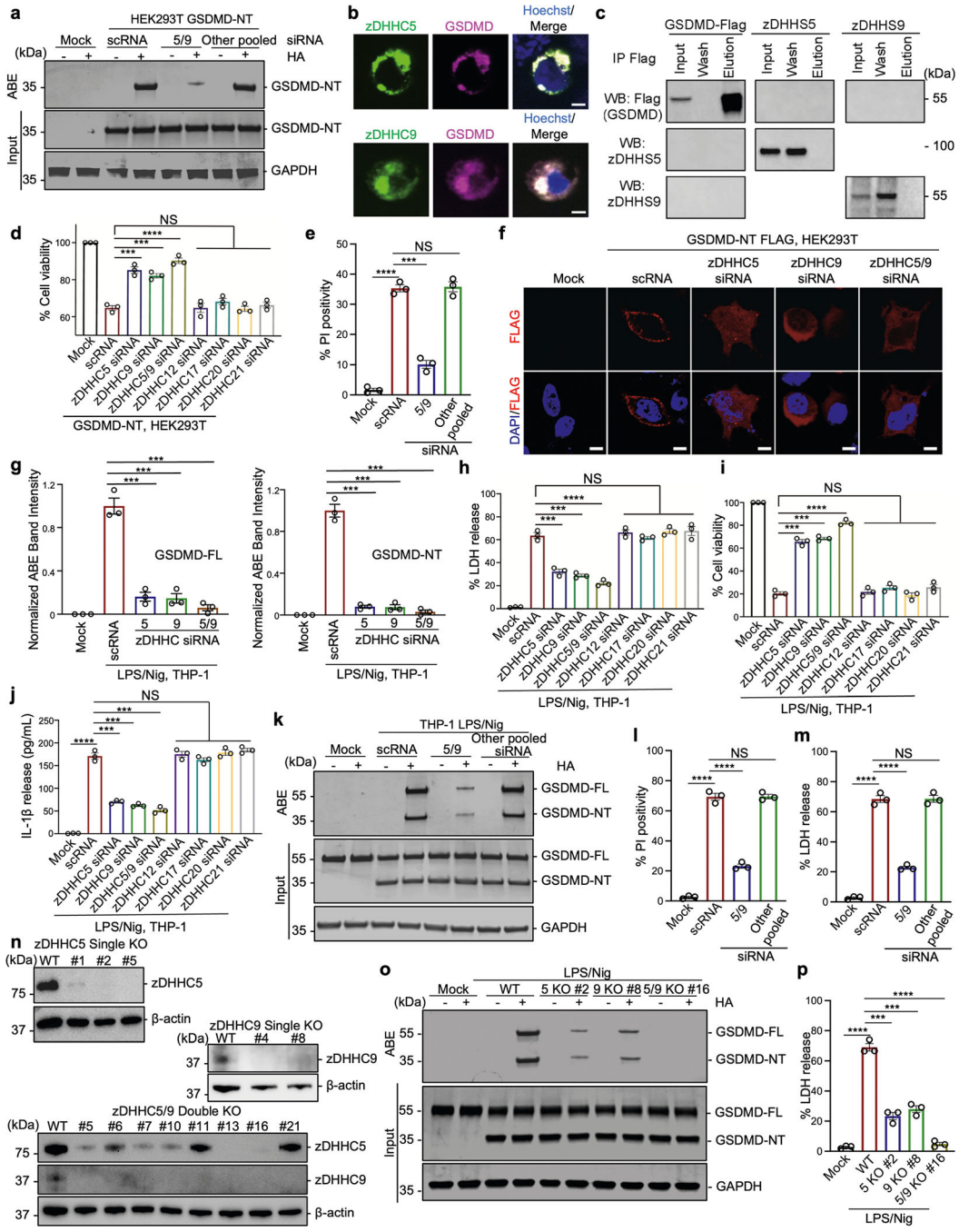

Extended Data Fig. 10 |. Identification of ZDHHC5 and ZDHHC9 as the main palmitoyltransferases for GSDMD palmitoylation and their regulation.

a, Palmitoylation as measured by ABE of GSDMD-NT expressed in HEK293T cells cotransfected with pooled siRNAs for *ZDHHC5* and *ZDHHC9*, or all human ZDHHCs except ZDHHC5/9. **b**, Co-localization imaging analysis of ZDHHC5-YFP and ZDHHC9-YFP with GSDMD-mCherry upon co-expression in HEK293T cells. Hoechst (blue) stained nuclei. The cap-like structures appear to be intact Golgi. Scale bars represent 5 μm. **c**, Anti-FLAG pulldown controls. ZDHHS5 and ZDHHS9 were not pulled down without co-

expression with the GSDMD-FLAG bait, and GSDMD-FLAG did not pull down ZDHHS5 and ZDHHS9 without the expression of ZDHHS5 and ZDHHS9. **d**,**e**, Cell viability (**d**), and PI positivity (**e**) of GSDMD-NT expressing HEK293T cells upon siRNA knockdowns of ZDHHCs. Other pooled siRNA contained siRNAs for all human ZDHHCs except ZDHHC5/9. **f**, Anti-FLAG immunofluorescence imaging of HEK293T cells with siRNA knockdowns of ZDHHC5, ZDHHC9, or both expressing GSDMD-NT-FLAG. Only cells treated with scRNA showed strong cell surface staining. Nuclei are marked by the DNA dye DAPI. Scale bars represent 5 μm. **g**, Quantification of GSDMD palmitoylation in Fig. 5f detected by ABE in THP-1 cells upon siRNA knockdown of ZDHHC5, ZDHHC9, or both and treatment with LPS plus nigericin, showing that these knockdowns compromised GSDMD palmitoylation. **h**-**j**, LDH release (**h**), cell viability (**i**), and IL-1β release (**j**) of THP-1 cells upon siRNA knockdown of ZDHHC5, ZDHHC9, both, or other ZDHHCs and treatment with LPS plus nigericin. **k**-**m**, Palmitoylation as measured by ABE of GSDMD (**k**), PI positivity (**l**) and LDH release (**m**) of WT THP-1 cells in the presence of pooled siRNAs for ZDHHC5 and ZDHHC9, or all human ZDHHCs except ZDHHC5/9. **n**, Western blots of THP-1 cells with single and double knockouts of ZDHHC5 or ZDHHC9, or both. **o**,**p**, Palmitoylation (**o**), and LDH release (**p**) of ZDHHC knockout THP-1 cell clones primed and activated with LPS and nigericin. All results were obtained from at least 3 independent experiments. Error bars represent SEM. Statistics were measured by two-tailed Student's t-tests with NS (non-significant) for $p > 0.05$, *** for $p < 0.001$, and **** for $p < 0.0001$. Immunoblots were incubated 1:1000 anti-FLAG® M2-peroxidase (HRP) antibody (**a**, **c**), 1:5000 anti-GAPDH antibody for GAPDH (**a**, **k**, **o**), 1:1000 anti-ZDHHC5 antibody (**c**), 1:1000 anti-ZDHHC9 antibody (**c**), 1:500 anti-ZDHHC5 antibody (**n**), 1:500 anti-ZDHHC9 antibody (**n**), 1:1000 anti-β-actin antibody (**n**), and 1:1000 anti-GSDMD antibody (**k**, **o**).

Supplementary Material

Refer to Web version on PubMed Central for supplementary material.

Acknowledgements

We thank D. Bachovchin for *GSDMD*-KO THP-1 cells, C. Serhan for suggestions for UPLC-MS/MS, the staff at Harvard Medical School Nikon Imaging Center for help with fluorescence microscopy and K. Durbin and the team at Proteinaceous for their ongoing assistance with TD Validator and Prosight Native. The graphical diagram was created using BioRender. This work was supported by US National Institutes of Health grants AI139914 (to H.W. and J.L.), HD087988 (to H.W.), AI124491 (to H.W.), CA240955 (to J.L.), AT010268 (to S.F.O.), AI167993 (to J.C.K.), AI116550 (to J.C.K.) and DK34854 (to J.C.K.). C.W. received a postdoctoral fellowship from NIGMS. P.D. was supported by a PhD Fellowship by the Boehringer Ingelheim Fonds. X.P. received a postdoctoral fellowship from the Cancer Research Institute. P.F. received a postdoctoral fellowship from the Cancer Research Institute. Y.D. received a postdoctoral fellowship from the Charles A. King Trust. T.J.E.-B. is an EP Abraham Junior Research Fellow at Linacre College. C.A.L. is a Research Fellow at Wolfson College.

Data availability

The RNA-seq data supporting the findings of this study have been deposited at Sequence Read Archive BioProject accession PRJNA1054142 (corresponding to data in Supplementary Fig. 5c–e). The cryo-EM density maps of full-length GSDMD and the 33-fold symmetric full-length GSDMD pore have been deposited at the Electron Microscopy Data Bank under accession numbers EMD-44035 and EMD-44034, respectively. All other

data are available from the corresponding authors on reasonable request. Source data are provided with this paper.

References

1. Kayagaki N et al. Caspase-11 cleaves gasdermin D for non-canonical inflammasome signalling. Nature 526, 666–671 (2015). [PubMed: 26375259]
2. Shi J et al. Cleavage of GSDMD by inflammatory caspases determines pyroptotic cell death. Nature 526, 660–665 (2015). [PubMed: 26375003]
3. Liu X et al. Inflammasome-activated gasdermin D causes pyroptosis by forming membrane pores. Nature 535, 153–158 (2016). [PubMed: 27383986]
4. Ding J et al. Pore-forming activity and structural autoinhibition of the gasdermin family. Nature 535, 111–116 (2016). [PubMed: 27281216]
5. Gaidt MM & Hornung V The NLRP3 inflammasome renders cell death pro-inflammatory. J. Mol. Biol. 430, 133–141 (2018). [PubMed: 29203171]
6. Broz P & Dixit VM Inflammasomes: mechanism of assembly, regulation and signalling. Nat. Rev. Immunol. 16, 407–420 (2016). [PubMed: 27291964]
7. Ruan J, Xia S, Liu X, Lieberman J & Wu H Cryo-EM structure of the gasdermin A3 membrane pore. Nature 557, 62–67 (2018). [PubMed: 29695864]
8. Xia S et al. Gasdermin D pore structure reveals preferential release of mature interleukin-1. Nature 593, 607–611 (2021). [PubMed: 33883744]
9. Liu X, Xia S, Zhang Z, Wu H & Lieberman J Channelling inflammation: gasdermins in physiology and disease. Nat. Rev. Drug Discov. 20, 384–405 (2021). [PubMed: 33692549]
10. Shi J, Gao W & Shao F Pyroptosis: gasdermin-mediated programmed necrotic cell death. Trends Biochem. Sci. 42, 245–254 (2017). [PubMed: 27932073]
11. Deng W et al. Streptococcal pyrogenic exotoxin B cleaves GSDMA and triggers pyroptosis. Nature 602, 496–502 (2022). [PubMed: 35110732]
12. Liu Z et al. Crystal structures of the full-length murine and human gasdermin d reveal mechanisms of autoinhibition, lipid binding, and oligomerization. Immunity 51, 43–49 (2019). [PubMed: 31097341]
13. Jiang H et al. Protein lipidation: occurrence, mechanisms, biological functions, and enabling technologies. Chem. Rev. 118, 919–988 (2018). [PubMed: 29292991]
14. Mesquita FS et al. Mechanisms and functions of protein *S*-acylation. Nat. Rev. Mol. Cell Biol. 10.1038/s41580-024-00700-8 (2024).
15. Schieber M & Chandel NS ROS function in redox signaling and oxidative stress. Curr. Biol. 24, R453–R462 (2014). [PubMed: 24845678]
16. Sobocinska J, Roszczenko-Jasinska P, Ciesielska A & Kwiatkowska K Protein palmitoylation and its role in bacterial and viral infections. Front. Immunol. 8, 2003 (2017). [PubMed: 29403483]
17. Davda D et al. Profiling targets of the irreversible palmitoylation inhibitor 2-bromopalmitate. ACS Chem. Biol. 8, 1912–1917 (2013). [PubMed: 23844586]
18. Xie Y et al. GPS-Lipid: a robust tool for the prediction of multiple lipid modification sites. Sci. Rep. 6, 28249 (2016). [PubMed: 27306108]
19. Hu L et al. Chemotherapy-induced pyroptosis is mediated by BAK/BAX-caspase-3-GSDME pathway and inhibited by 2-bromopalmitate. Cell Death Dis. 11, 281 (2020). [PubMed: 32332857]
20. Aglietti RA et al. GsdmD p30 elicited by caspase-11 during pyroptosis forms pores in membranes. Proc. Natl Acad. Sci. USA 113, 7858–7863 (2016). [PubMed: 27339137]
21. Sorek N & Yalovsky S Analysis of protein *S*-acylation by gas chromatography-coupled mass spectrometry using purified proteins. Nat. Protoc. 5, 834–840 (2010). [PubMed: 20379138]
22. Ji Y et al. Direct detection of *S*-palmitoylation by mass spectrometry. Anal. Chem. 85, 11952–11959 (2013). [PubMed: 24279456]
23. Devant P et al. Gasdermin D pore-forming activity is redox-sensitive. Cell Rep. 42, 112008 (2023). [PubMed: 36662620]

24. Evavold CL et al. Control of gasdermin D oligomerization and pyroptosis by the Ragulator-Rag-mTORC1 pathway. Cell 184, 4495–4511 (2021). [PubMed: 34289345]
25. Johnson AG et al. Bacterial gasdermins reveal an ancient mechanism of cell death. Science 375, 221–225 (2022). [PubMed: 35025633]
26. Gritsenko A et al. Priming is dispensable for NLRP3 inflammasome activation in human monocytes in vitro. Front. Immunol. 11, 565924 (2020). [PubMed: 33101286]
27. Zhou R, Yazdi AS, Menu P & Tschopp J A role for mitochondria in NLRP3 inflammasome activation. Nature 469, 221–225 (2011). [PubMed: 21124315]
28. Zhuang Z, Gu J, Li BO & Yang L Inhibition of gasdermin D palmitoylation by disulfiram is crucial for the treatment of myocardial infarction. Transl. Res. 264, 66–75 (2024). [PubMed: 37769810]
29. Saurin AT, Neubert H, Brennan JP & Eaton P Widespread sulfenic acid formation in tissues in response to hydrogen peroxide. Proc. Natl Acad. Sci. USA 101, 17982–17987 (2004). [PubMed: 15604151]
30. Munoz-Planillo R et al. K^+ efflux is the common trigger of NLRP3 inflammasome activation by bacterial toxins and particulate matter. Immunity 38, 1142–1153 (2013). [PubMed: 23809161]
31. Zhang P et al. NLRC4 inflammasome-dependent cell death occurs by a complementary series of three death pathways and determines lethality in mice. Sci. Adv. 7, eabi9471 (2021). [PubMed: 34678072]
32. Miao R et al. Gasdermin D permeabilization of mitochondrial inner and outer membranes accelerates and enhances pyroptosis. Immunity 56, 2523–2541 (2023). [PubMed: 37924812]
33. Chen D, Zhang XY & Shi Y Identification and functional characterization of hCLS1, a human cardiolipin synthase localized in mitochondria. Biochem. J. 398, 169–176 (2006). [PubMed: 16716149]
34. Horvath SE & Daum G Lipids of mitochondria. Prog. Lipid Res. 52, 590–614 (2013). [PubMed: 24007978]
35. Dudek J Role of cardiolipin in mitochondrial signaling pathways. Front. Cell Dev. Biol. 5, 90 (2017). [PubMed: 29034233]
36. Chu CT et al. Cardiolipin externalization to the outer mitochondrial membrane acts as an elimination signal for mitophagy in neuronal cells. Nat. Cell Biol. 15, 1197–1205 (2013). [PubMed: 24036476]
37. de Kroon AI, Dolis D, Mayer A, Lill R & de Kruijff B Phospholipid composition of highly purified mitochondrial outer membranes of rat liver and *Neurospora crassa*. Is cardiolipin present in the mitochondrial outer membrane? Biochim. Biophys. Acta 1325, 108–116 (1997). [PubMed: 9106488]
38. Liu J et al. Phospholipid scramblase 3 controls mitochondrial structure, function, and apoptotic response. Mol. Cancer Res. 1, 892–902 (2003). [PubMed: 14573790]
39. Zhou X et al. Integrating de novo and inherited variants in 42,607 autism cases identifies mutations in new moderate-risk genes. Nat. Genet. 54, 1305–1319 (2022). [PubMed: 35982159]
40. Lanigan TM et al. Real time visualization of cancer cell death, survival and proliferation using fluorochrome-transfected cells in an IncuCyte((R)) imaging system. J Biol Methods 7, e133 (2020). [PubMed: 32577423]
41. Puthenveetil R et al. *S*-acylation of SARS-CoV-2 spike protein: mechanistic dissection, in vitro reconstitution and role in viral infectivity. J. Biol. Chem. 297, 101112 (2021). [PubMed: 34428449]
42. Ko PJ et al. A ZDHHC5-GOLGA7 protein acyltransferase complex promotes nonapoptotic cell death. Cell Chem. Biol. 26, 1716–1724 (2019). [PubMed: 31631010]
43. Orre LM et al. SubCellBarCode: proteome-wide mapping of protein localization and relocalization. Mol Cell 73, 166–182 (2019). [PubMed: 30609389]
44. Hao JW et al. CD36 facilitates fatty acid uptake by dynamic palmitoylation-regulated endocytosis. Nat. Commun. 11, 4765 (2020). [PubMed: 32958780]
45. Shimell JJ et al. The X-linked intellectual disability gene Zdhhc9 Is essential for dendrite outgrowth and inhibitory synapse formation. Cell Rep. 29, 2422–2437 (2019). [PubMed: 31747610]

46. Rathkey JK et al. Chemical disruption of the pyroptotic pore-forming protein gasdermin D inhibits inflammatory cell death and sepsis. Sci. Immunol. 3, eaat2738 (2018). [PubMed: 30143556]
47. Hu JJ et al. FDA-approved disulfiram inhibits pyroptosis by blocking gasdermin D pore formation. Nat. Immunol. 21, 736–745 (2020). [PubMed: 32367036]
48. Humphries F et al. Succination inactivates gasdermin D and blocks pyroptosis. Science 369, 1633–1637 (2020). [PubMed: 32820063]
49. Mesquita FS et al. *S*-acylation controls SARS-CoV-2 membrane lipid organization and enhances infectivity. Dev. Cell 56, 2790–2807 (2021). [PubMed: 34599882]
50. Percher A, Thinon E & Hang H Mass-tag labeling using acyl-PEG exchange for the determination of endogenous protein *S*-fatty acylation. Curr. Protoc. Protein Sci. 89, 14.17.11–14.17.11 (2017).
51. Okondo MC et al. Inhibition of Dpp8/9 activates the Nlrp1b inflammasome. Cell Chem. Biol. 25, 262–267 (2018). [PubMed: 29396289]
52. Marim FM, Silveira TN, Lima DS Jr & Zamboni DS A method for generation of bone marrow-derived macrophages from cryopreserved mouse bone marrow cells. PLoS ONE 5, e15263 (2010). [PubMed: 21179419]
53. Liu Z et al. Caspase-1 engages full-length gasdermin D through two distinct interfaces that mediate caspase recruitment and substrate cleavage. Immunity 53, 106–114 (2020). [PubMed: 32553275]
54. Brigidi GS & Bamji SX Detection of protein palmitoylation in cultured hippocampal neurons by immunoprecipitation and acyl-biotin exchange (ABE). J. Vis. Exp. (2013).
55. Love MI, Huber W & Anders S Moderated estimation of fold change and dispersion for RNA-seq data with DESeq2. Genome Biol. 15, 550 (2014). [PubMed: 25516281]
56. Sanjana NE, Shalem O & Zhang F Improved vectors and genome-wide libraries for CRISPR screening. Nat. Methods 11, 783–784 (2014). [PubMed: 25075903]
57. Zhang Y et al. BAP1 links metabolic regulation of ferroptosis to tumour suppression. Nat. Cell Biol. 20, 1181–1192 (2018). [PubMed: 30202049]
58. Gault J et al. High-resolution mass spectrometry of small molecules bound to membrane proteins. Nat. Methods 13, 333–336 (2016). [PubMed: 26901650]
59. Durbin KR et al. ProSight native: defining protein complex composition from native top-down mass spectrometry data. J. Proteome Res. 22, 2660–2668 (2023). [PubMed: 37436406]
60. Fornelli L et al. Accurate sequence analysis of a monoclonal antibody by top-down and middle-down orbitrap mass spectrometry applying multiple ion activation techniques. Anal. Chem. 90, 8421–8429 (2018). [PubMed: 29894161]
61. von Moltke J et al. Rapid induction of inflammatory lipid mediators by the inflammasome in vivo. Nature 490, 107–111 (2012). [PubMed: 22902502]
62. Mastronarde DN Automated electron microscope tomography using robust prediction of specimen movements. J. Struct. Biol. 152, 36–51 (2005). [PubMed: 16182563]
63. Morin A et al. Collaboration gets the most out of software. eLife 2, e01456 (2013). [PubMed: 24040512]
64. Punjani A, Rubinstein JL, Fleet DJ & Brubaker MA cryoSPARC: algorithms for rapid unsupervised cryo-EM structure determination. Nat. Methods 14, 290–296 (2017). [PubMed: 28165473]
65. Goddard TD et al. UCSF ChimeraX: meeting modern challenges in visualization and analysis. Protein Sci. 27, 14–25 (2018). [PubMed: 28710774]
66. Zivanov J et al. New tools for automated high-resolution cryo-EM structure determination in RELION-3. eLife 7, e42166 (2018). [PubMed: 30412051]
67. Zheng SQ et al. MotionCor2: anisotropic correction of beam-induced motion for improved cryo-electron microscopy. Nat. Methods 14, 331–332 (2017). [PubMed: 28250466]
68. Delano WL The PyMol Molecular Graphics System. (Delano Scientific, 2002).
69. Baroni L, Abreu-Filho PG, Pereira LM, Nagl M & Yatsuda AP Recombinant actin-depolymerizing factor of the apicomplexan Neospora caninum (NcADF) is susceptible to oxidation. Front. Cell Infect. Microbiol. 12, 952720 (2022). [PubMed: 36601306]
70. Roschitzki-Voser H et al. Human caspases in vitro: expression, purification and kinetic characterization. Protein Expr. Purif. 84, 236–246 (2012). [PubMed: 22683476]

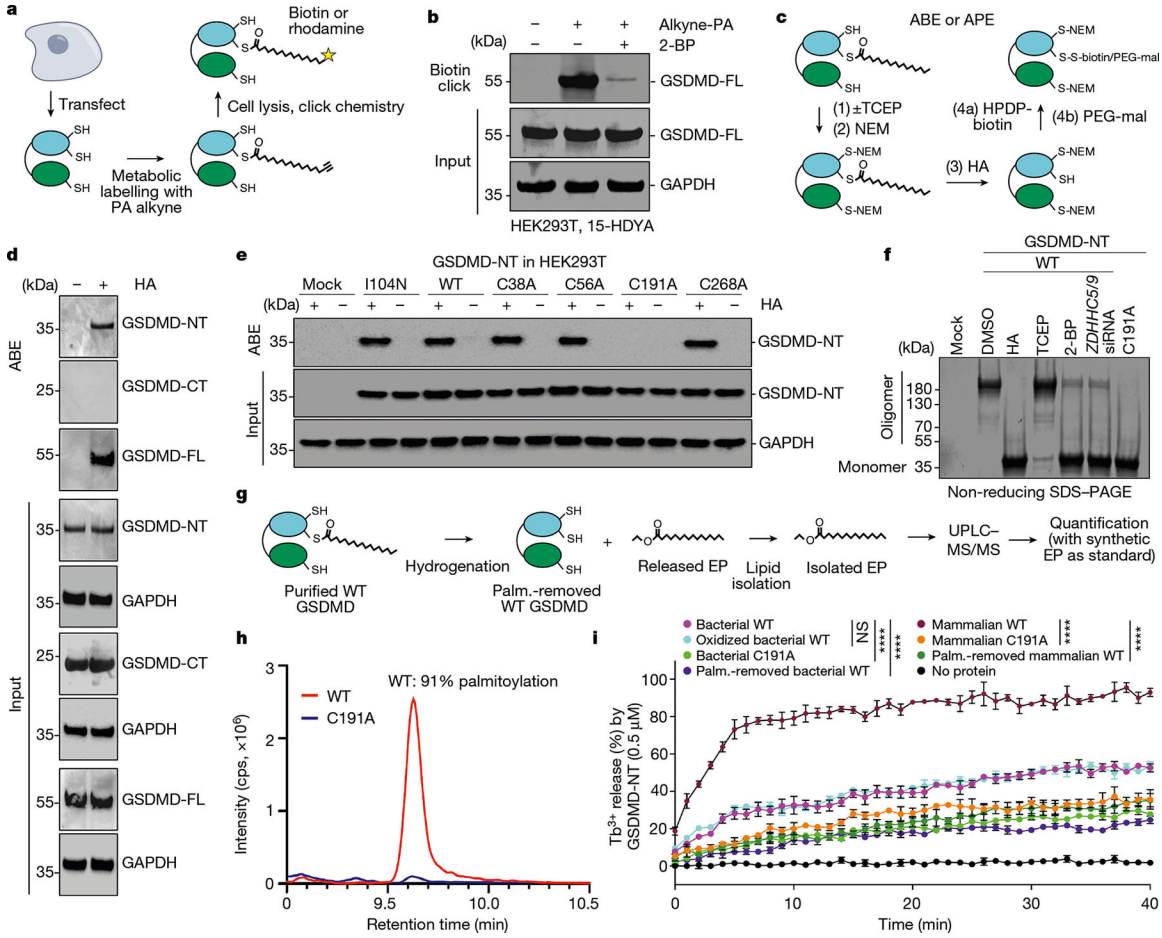

Fig. 1 |. GSDMD is palmitoylated as detected using three methods, with 2-BP and C191A inhibiting palmitoylation.

a, Schematic of metabolic labelling and click chemistry for detecting protein modification by palmitic acid (PA). GSDMD-NT and GSDMD-CT are shown as ovals in cyan and green. The yellow star denotes biotin or rhodamine. **b**, Full-length GSDMD palmitoylation when expressed in HEK293T cells, detected by alkyne-PA labelling, biotin–azide click, and biotin pull-down, and its inhibition by palmitoylation inhibitor 2-BP. **c**, Schematic of ABE or APE for detecting protein acylation. NEM, *N*-ethylmaleimide. **d**, Palmitoylation of full-length GSDMD and GSDMD-NT, but not GSDMD-CT. **e**, Palmitoylation of WT GSDMD-NT and Cys mutants of GSDMD-NT; only C191A mutant was defective in palmitoylation. **f**, Non-reducing SDS–PAGE and western blot analysis of WT or C191A GSDMD-NT when expressed in HEK293T cells. WT GSDMD-NT lysates were untreated, treated with HA to break acylation, treated with TCEP to break disulfide bonds or reduce oxidation, pretreated with 2-BP, or co-expressed with siRNAs to knockdown *ZDHHC5* and *ZDHHC9*, which mediate GSDMD palmitoylation. Cells were treated with the ROS activator ROT to increase palmitoylation. **g**, Schematic of quantitative palmitoylation (palm.) detection using ultra-high performance liquid chromatography coupled to tandem MS (UPLC–MS/MS). **h**, UPLC peaks during the UPLC–MS/MS analysis of released EP from purified WT and C191A GSDMD expressed in Expi293 cells under treatment with ROT. WT GSDMD palmitoylation was detected at 91%, whereas GSDMD (C191A) palmitoylation was not

detected. cps, counts per second. **i**, The rate of liposome leakage for Expi293-cell-expressed palmitoylated GSDMD-NT compared with HA-treated depalmitoylated GSDMD-NT or GSDMD (C191A). Data are mean ± s.e.m. $n = 3$. Statistical analysis was performed using two-way analysis of variance (ANOVA); not significant (NS), $P > 0.05$; **** $P < 0.0001$. Representative of at least three independent experiments (**b** and **d**–**f**). Immunoblots were incubated with anti-Flag M2-peroxidase (HRP; 1:1,000) for GSDMs and anti-GAPDH (1:5,000; loading control) antibodies.

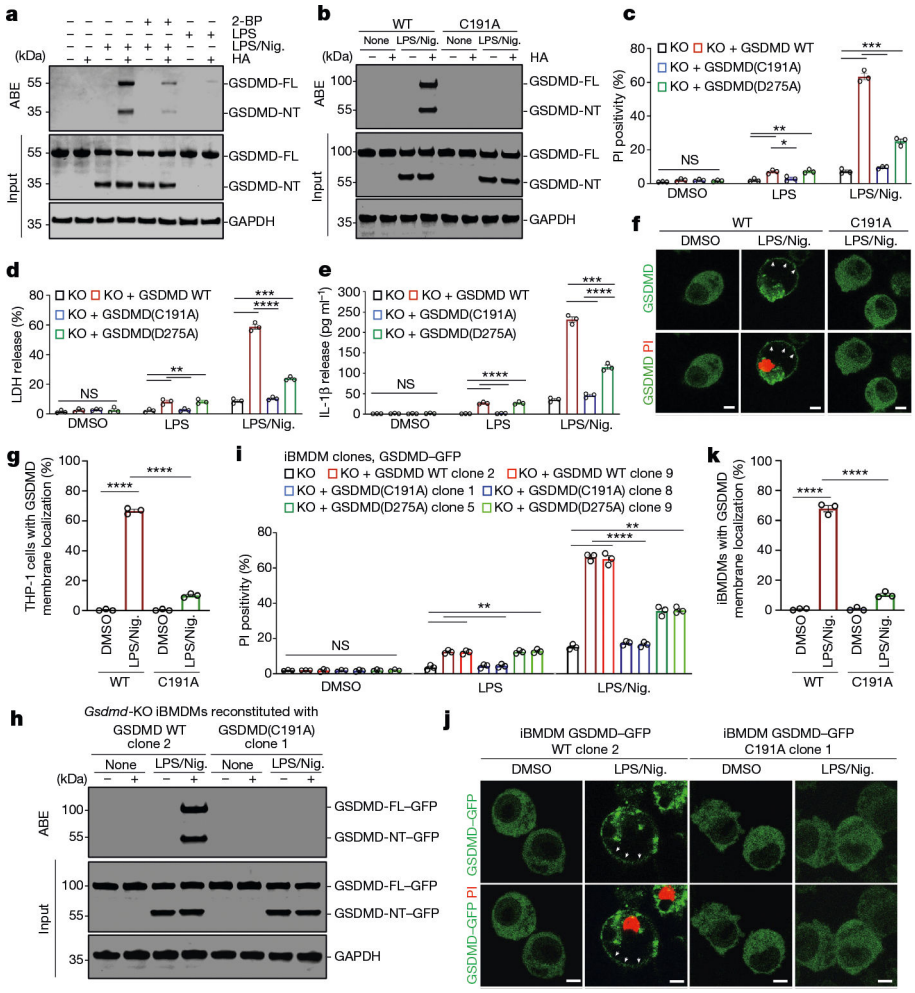

Fig. 2 |. GSDMD palmitoylation during inflammasome activation, and the functional effects of palmitoylation-defective C191A and cleavage-deficient D275A mutants.

a, Palmitoylation of full-length GSDMD and GSDMD-NT in THP-1 cells after priming and activation. 2-BP inhibited GSDMD palmitoylation without affecting processing. **b**–**e**, Palmitoylation (**b**), PI positivity (**c**), LDH release (**d**) and IL-1β release (**e**) in *GSDMD*-KO THP-1 cells reconstituted with WT, C191A or cleavage-deficient D275A GSDMD–GFP. GSDMD(C191A) was defective in cell death after treatment by LPS and nigericin, whereas GSDMD(D275A) was partially functional despite the lack of cleavage. **f**,**g**, Representative images (**f**) and quantification (**g**) of GSDMD membrane localization in *GSDMD*-KO THP-1 cells that were reconstituted with WT or C191A GSDMD–GFP after priming and activation. Membrane localization was seen for WT GSDMD-reconstituted cells with substantially reduced membrane localization in GSDMD(C191A)-reconstituted cells. **h**, Palmitoylated GSDMD was detected by ABE in *Gsdmd*-KO iBMDMs that were reconstituted with WT or C191A GSDMD–GFP. **i**, PI positivity of *Gsdmd*-KO iBMDMs reconstituted with WT, C191A or D275A GSDMD–GFP after priming and activation. **j**,**k**, Representative images (**j**) and quantification (**k**) of GSDMD membrane localization in *Gsdmd*-KO iBMDMs that were reconstituted with WT or C191A GSDMD–GFP. For **f** and **j**, PI staining marks cell death; and the arrow heads indicate pyroptotic bubbles. Scale bars, 5 μm (**f** and **j**). All results were

obtained from at least three independent experiments. Expression levels of GSDMD–GFP in reconstituted THP-1 cells were equal to endogenous GSDMD in WT THP-1 cells (**b**–**g**). Clones of GSDMD–GFP-reconstituted iBMDMs with equal expression levels to endogenous GSDMD in WT iBMDMs were selected (**h**–**k**). Data are mean ± s.e.m. For **c**–**e**, **g**, **i** and **k**, statistical analysis was performed using two-tailed Student's *t*-tests; $*P < 0.05$, $**P < 0.01$, $***P < 0.001$. Immunoblots were incubated with anti-GSDMD (1:1,000) and anti-GAPDH (loading control; 1:5,000) antibodies.

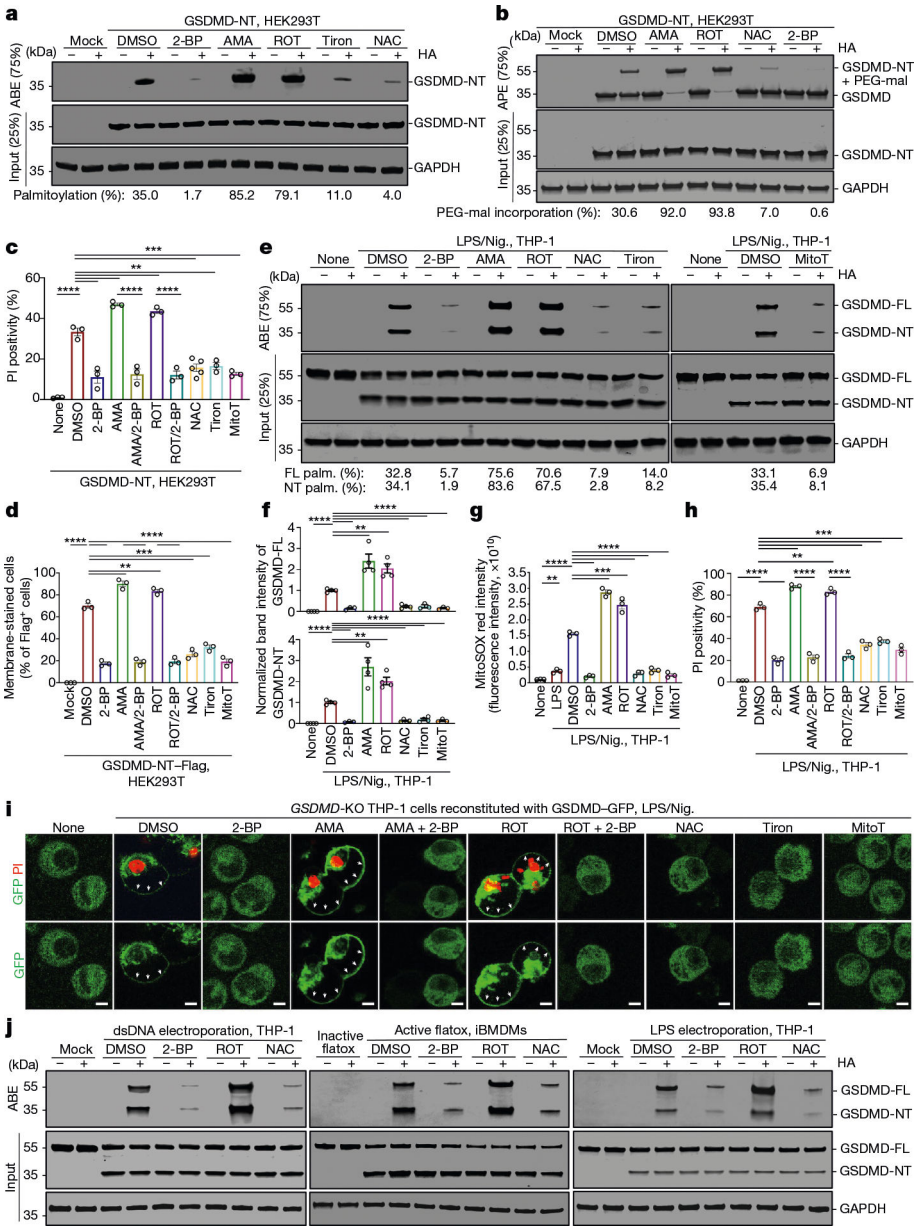

Fig. 3 |. Regulation of GSDMD palmitoylation and pyroptosis by ROS modulators.

a,**b**, Quantification of GSDMD-NT palmitoylation using ABE (**a**) or APE (**b**) in HEK293T cells treated with the ROS activators ROT or AMA, or the ROS quenchers Tiron, NAC or MitoT. Although the PEG-mal used was 10 kDa in size, the molecular mass shift that it caused is approximately twice this size, as noted previously[50]. **c**,**d**, PI positivity (**c**) and membrane staining (**d**) of HEK293T cells expressing GSDMD-NT–Flag treated with ROS modulators, showing enhanced pyroptosis after treatment with ROT and AMA, and decreased pyroptosis after treatment with NAC, Tiron and NAC. **e**,**f**, Full-length GSDMD and GSDMD-NT palmitoylation (**e**) and quantification (**f**) was detected by ABE in THP-1 cells after activation by LPS and nigericin and treatment with ROS activators or quenchers. **g**,**h**, MitoSOX red intensity (**g**) and PI positivity (**h**) in THP-1 cells after activation by LPS

and nigericin and treatment with ROS inducers or quenchers. **i**, Representative fluorescence microscopy images of *GSDMD*-KO THP-1 cells that were reconstituted with WT GSDMD–GFP after activation by LPS and nigericin and treated with ROS inducers or quenchers or 2-BP, showing enhanced GSDMD membrane localization by inflammasome activation and ROS activators, and inhibition by ROS quenchers and 2-BP. Expression levels of GSDMD–GFP in reconstituted THP-1 cells were equal to endogenous GSDMD in WT THP-1 cells. Scale bars, 5 μm. The arrowheads indicate pyroptotic bubbles. **j**, GSDMD palmitoylation detected by ABE in THP-1 cells or iBMDMs after activation of various inflammasomes, and after treatment with ROS activator ROT, ROS quencher NAC or 2-BP. All results were obtained from at least three independent experiments. Data are mean ±s.e.m. Statistical analysis was performed using two-tailed Student's *t*-tests. Immunoblots were incubated with anti-Flag M2-peroxidase (HRP; 1:1,000; **a** and **b**), anti-GSDMD (1:1,000; **e** and **j**) and anti-GAPDH (1:5,000; loading controls) antibodies.

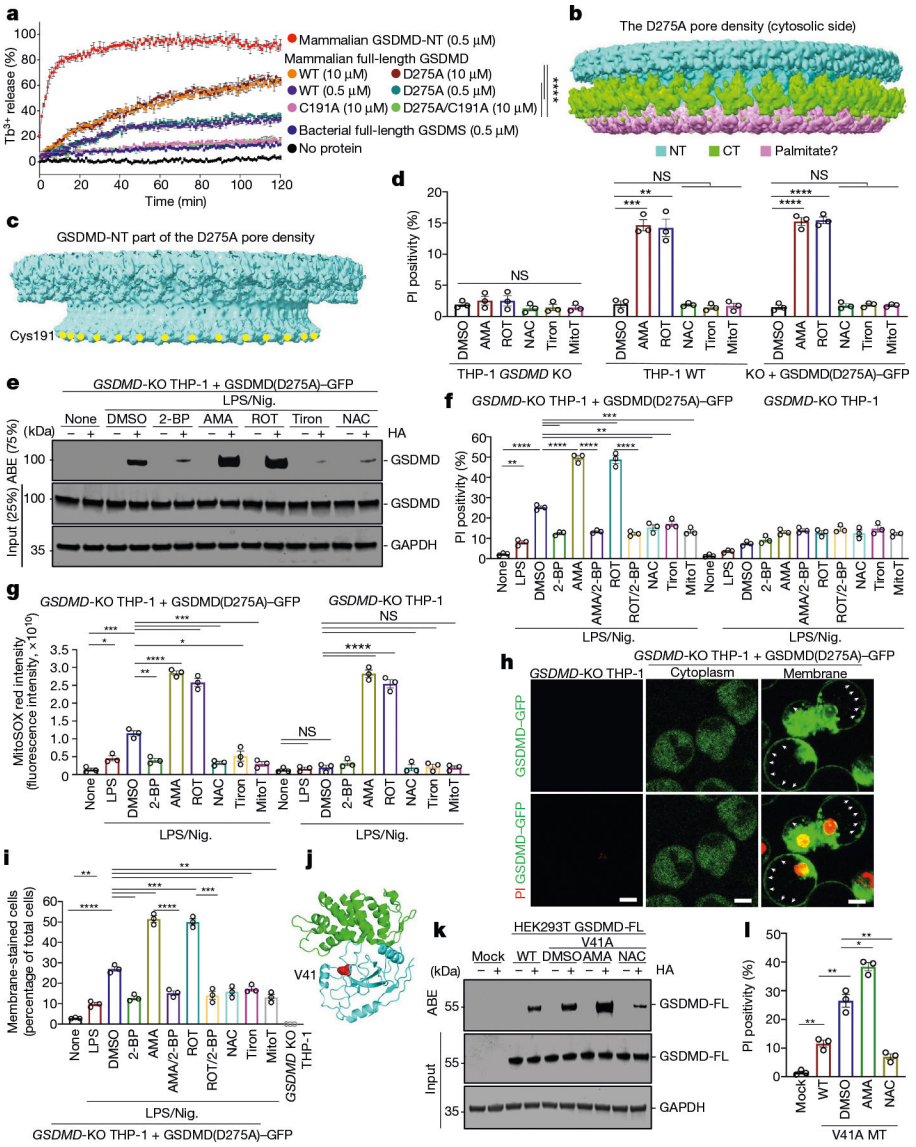

Fig. 4 |. Palmitoylated intact GSDMD can form active full-length pores and induce pyroptosis.

a, Liposome leakage assay of Expi293-cell-expressed intact GSDMD WT, GSDMD(D275A), GSDMD(C191A) and GSDMD(D275A/C191A). Bacterially expressed intact GSDMD and Expi293-cell-expressed cleaved GSDMD were used as positive and negative controls. **b**, Overall view of the cryo-EM density segmented to show GSDMD-NT (cyan), the probable region for GSDMD-CT (green) and the probable region for palmitate (magenta). **c**, The GSDMD-NT part of the full-length GSDMD pore density; the location of Cys191 is coloured in yellow. **d**, ROS activators alone induced significant cell death in WT THP-1 and *GSDMD*-KO THP-1 cells that were reconstituted with the GSDMD(D275A)–GFP uncleavable mutant. **e**–**g**, Palmitoylation (**e**), PI positivity (**f**) and MitoSOX intensity (**g**) in *GSDMD*-KO THP-1 cells that were reconstituted with GSDMD(D275A)–GFP, activated by LPS and nigericin, and treated with ROS activators, quenchers or 2-BP. **h**,**i**, *GSDMD*-KO THP-1 cells that were reconstituted with GSDMD(D275A)–GFP imaged with GFP and PI (**h**) and quantified (**i**). Scale bars, 5 μm (**h**). The arrowheads indicate pyroptotic

bubbles. **j**, The structure of unpalmitoylated GSDMD (Protein Data Bank (PDB): 6N9O) with NT (cyan), CT (green) and Val41 at the NT–CT interface (red) highlighted. The autism-associated V41A mutation probably overcomes autoinhibition. **k**,**l**, Palmitoylation (**k**) and PI positivity (**l**) of HEK293T cells expressing the full-length GSDMD(V41A) autism-associated mutant and treated with ROS modulators showing enhanced pyroptosis by ROT and AMA, and decreased pyroptosis by NAC. The V41A autism-associated mutant has increased cell death compared with WT full-length GSDMD. All results were obtained from at least three independent experiments. Data are mean ± s.e.m. Statistical analysis was performed using two-tailed Student's *t*-tests (**d**, **f**, **g**, **i** and **l**) and two-way ANOVA (**a**). Immunoblots were incubated anti-GSDMD (**e**; 1:1,000), anti-Flag M2-peroxidase (HRP; 1:1,000) for GSDMD (**k**) and anti-GAPDH (loading controls; 1:5,000) antibodies.

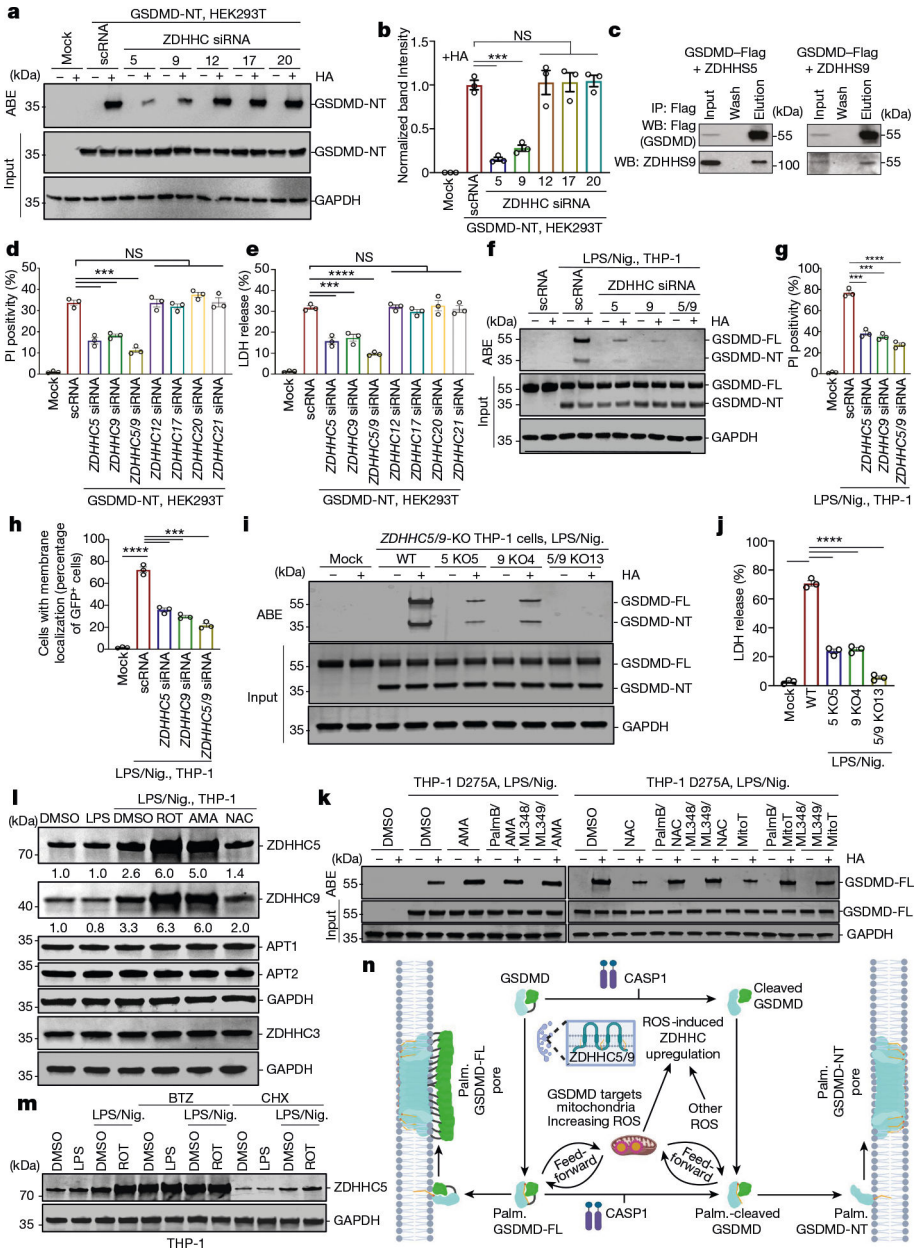

Fig. 5 |. Identification of ZDHHC5 and ZDHHC9 as the main palmitoyltransferases for GSDMD palmitoylation.

a,**b**, Palmitoylation (**a**) and quantification (**b**) in HEK293T cells transfected with GSDMD-NT after siRNA knockdown of ZDHHCs. **c**, Anti-Flag pull-down of ZDHHS5 and ZDHHS9, co-expressed with GSDMD–Flag. IP, immunoprecipitation; WB, western blot. **d**,**e**, PI positivity (**d**) and LDH release (**e**) of GSDMD-NT-expressing HEK293T cells after siRNA knockdown of ZDHHCs. **f**, GSDMD palmitoylation in THP-1 cells after siRNA knockdown of ZDHHCs and treatment with LPS plus nigericin. **g**,**h**, PI positivity (**g**) and membrane localization (**h**) of THP-1 cells after siRNA knockdown of ZDHHCs and after priming and activation. **i**,**j**, Palmitoylation (**i**) and LDH release (**j**) of THP-1 clones with CRISPR–Cas9 knockout of *ZDHHC5*, *ZDHHC9* or both. **k**, GSDMD palmitoylation in

GSDMD-KO THP-1 cells reconstituted with GSDMD(D275A) pretreated with palmostatin B (PalmB), ML348/ML349 together, a ROS modulator, or LPS and nigericin. **l**, The expression levels of ZDHHC3/5/9 and APT1/2 in THP-1 cells treated with LPS, LPS plus nigericin, or LPS plus nigericin with ROS modulators. Quantified band intensities are shown for ZDHHC5 and ZDHHC9. **m**, The expression level of ZDHHC5 in THP-1 cells treated with LPS, LPS plus nigericin, LPS plus nigericin treated with ROT, or additionally treated with the proteasome inhibitor BTZ or protein translation inhibitor CHX. **n**, The proposed model for how palmitoylation enhances GSDMD-NT and full-length GSDMD pore formation. All results were obtained from at least three independent experiments. The schematic in **n** was created using BioRender. Data are mean ± s.e.m. Statistical analysis was performed using two-tailed Student's *t*-tests. Immunoblots were incubated with anti-Flag M2-peroxidase (HRP; 1:1,000; **a** and **c**), anti-ZDHHC5 (1:1,000) and anti-ZDHHC9 (1:1,000; **c**); anti-ZDHHC5 (1:500) and anti-ZDHHC9 (1:500; **l** and **m**); anti-GSDMD (1:1,000; **f**, **i** and **k**); anti-APT1 (1:1,000) and anti-APT2 (1:1,000; **l**); anti-ZDHHC3 (1:1,000; **l**); and anti-GAPDH (1:5,000; loading controls) antibodies.